NEUROSCIENCE

Human-specific features and developmental dynamics of the brain N-glycome

Thomas S. Klarić[1,2]†, Ivan Gudelj[1,2,3]†, Gabriel Santpere[1,4], Mislav Novokmet[2], Frano Vučković[2], Shaojie Ma[1], Hannah M. Doll[5,6], Ryan Risgaard[5,6], Shveta Bathla[7], Amir Karger[8], Angus C. Nairn[7], Victor Luria[1,9], Ivona Bečeheli[2], Chet C. Sherwood[10], John J. Ely[11,12], Patrick R. Hof[13], André M. M. Sousa[5,6], Djuro Josić[3,14], Gordan Lauc[2,15]*, Nenad Sestan[1,7,16]*

Comparative "omics" studies have revealed unique aspects of human neurobiology, yet an evolutionary perspective of the brain N-glycome is lacking. We performed multiregional characterization of rat, macaque, chimpanzee, and human brain N-glycomes using chromatography and mass spectrometry and then integrated these data with complementary glycotranscriptomic data. We found that, in primates, the brain N-glycome has diverged more rapidly than the underlying transcriptomic framework, providing a means for rapidly generating additional interspecies diversity. Our data suggest that brain N-glycome evolution in hominids has been characterized by an overall increase in complexity coupled with a shift toward increased usage of α(2-6)–linked *N*-acetylneuraminic acid. Moreover, interspecies differences in the cell type expression pattern of key glycogenes were identified, including some human-specific differences, which may underpin this evolutionary divergence. Last, by comparing the prenatal and adult human brain N-glycomes, we uncovered region-specific neurodevelopmental pathways that lead to distinct spatial N-glycosylation profiles in the mature brain.

INTRODUCTION

The human brain is an immensely complex organ and accordingly must undergo a protracted period of development before reaching maturity (*1*). There is an increasing desire to uncover the cellular and molecular evolutionary specializations that make the human brain, as well as its development, unique. The majority of our knowledge regarding such human-specific features has been derived from comparative "omics" studies involving humans and nonhuman primates at the genome, transcriptome, proteome, and metabolome level (*2*–*8*). However, the contribution of post-translational sugar modifications in generating interspecies molecular diversity has not been explored in the context of primate brain evolution.

Glycans are complex sugar chains that can be attached to other macromolecules, such as proteins, lipids, or RNA, and they mediate many important biological phenomena that occur at the cell surface, including functions critical to the host organism and interactions with pathogens. Consequently, the evolution of the glycome is uniquely driven by both intrinsic and extrinsic selection pressures (*9*). Asparagine-linked glycosylation (N-glycosylation) is a type of posttranslational modification in which nascent proteins are modified by the attachment of branched polysaccharides called N-glycans at specific asparagine residues located within conserved sequons. N-glycans are critically involved in many aspects of central nervous system (CNS) biology including membrane excitability, synaptic transmission, neurite outgrowth, and neuronal plasticity (*10*, *11*). Recent insights have revealed that the brain N-glycome is dynamic and that its composition changes under various physiological and pathological conditions (*12*), yet data regarding its evolutionary trajectory are scarce. Only a single comparative N-glycomics study has investigated interspecies differences in N-glycosylation at the whole N-glycome level, although it was limited to two species, mice and humans, and a single brain region (*13*). Moreover, no data exist regarding the neuroglycome of nonhuman primates. Consequently, we lack a holistic view of the evolutionary trends that have shaped the neuroglycome in primates.

Here, we performed a multiregional comparative N-glycomics study to define, as well as anatomically pinpoint, evolutionary specializations unique to primates with an emphasis on identifying human-specific features of brain N-glycosylation (Fig. 1A and fig. S1). Four species representing key phylogenetic groups within the Euarchontoglires branch of mammals were investigated: humans, chimpanzees, rhesus macaque monkeys, and rats. In each species, four functionally and cytoarchitecturally distinct brain regions (or their corresponding homologous equivalents) were investigated: the dorsolateral prefrontal cortex (DFC), hippocampus (HIP), striatum (STR), and cerebellar cortex (CBC). We performed detailed structural characterization of the brain N-glycomes using an ultraperformance liquid chromatography method based on hydrophilic

[1]Department of Neuroscience, Yale School of Medicine, New Haven, CT, USA. [2]Genos Glycoscience Research Laboratory, Zagreb, Croatia. [3]Department of Biotechnology, University of Rijeka, Rijeka, Croatia. [4]Hospital del Mar Research Institute, Barcelona, Catalonia, Spain. [5]Waisman Center and Department of Neuroscience, School of Medicine and Public Health, University of Wisconsin-Madison, Madison, WI, USA. [6]Department of Neuroscience, University of Wisconsin-Madison, Madison, WI, USA. [7]Department of Psychiatry, Yale School of Medicine, New Haven, CT, USA. [8]IT Research Computing, Harvard Medical School, Boston, MA, USA. [9]Division of Genetics and Genomics, Boston Children's Hospital, Harvard Medical School, Boston, USA. [10]Department of Anthropology, The George Washington University, Washington, DC, USA. [11]Center for the Advanced Study of Human Paleobiology, The George Washington University, Washington, DC, USA. [12]MAEBIOS, Alamogordo, NM, USA. [13]Nash Family Department of Neuroscience and Friedman Brain Institute, Icahn School of Medicine at Mount Sinai, New York, NY, USA. [14]Warren Alpert Medical School, Brown University, Providence, RI, USA. [15]University of Zagreb Faculty of Pharmacy and Biochemistry, Zagreb, Croatia. [16]Departments of Genetics and Comparative Medicine, Kavli Institute for Neuroscience, Program in Cellular Neuroscience, Neurodegeneration and Repair, and Yale Child Study Center, Yale School of Medicine, New Haven, CT, USA.
*Corresponding author. Email: nenad.sestan@yale.edu (N.S.); glauc@genos.hr (G.L.)
†These authors contributed equally to this work.

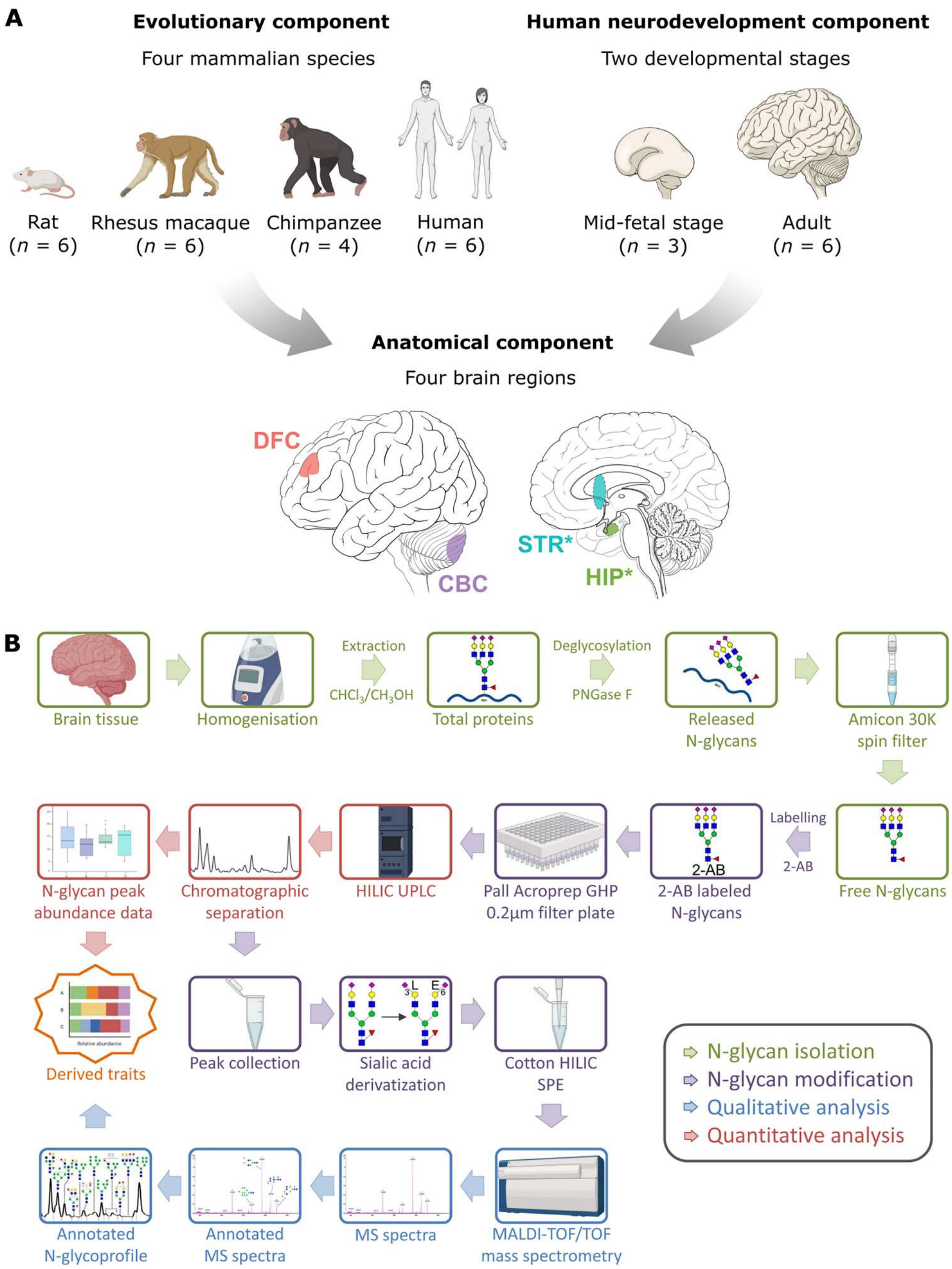

Fig. 1. Study design and workflow. (**A**) The mammalian species and developmental stages investigated in the evolutionary and neurodevelopmental components of the study, respectively. The same four brain regions (or their corresponding homologous or developmental equivalents) were analyzed from each specimen for the anatomical component. The number of individual animals or donors analyzed (i.e., the number of biological replicates) per group (*n*) is indicated. DFC, dorsolateral prefrontal cortex; HIP, hippocampus; STR, striatum; CBC, cerebellar cortex. *Denotes that regions are internal and not visible from the view shown. (**B**) Schematic of the laboratory workflow used for sample preparation and analysis. Linkage-specific derivatization of sialic acid by chemical modification resulted in enhanced stability of sialylated N-glycans in mass spectrometry and allowed for differentiation between lactonized α(2-3)–linked Neu5Ac (L) and esterified α(2-6)–linked Neu5Ac (E) based on mass difference. See Materials and Methods for details.

interactions (HILIC-UPLC) coupled with matrix-assisted laser desorption/ionization–time-of-flight/time-of-flight tandem mass spectrometry (MALDI-TOF/TOF-MS/MS; Fig. 1B and fig. S2). In addition, we then integrated these N-glycomics data with complementary tissue and single-nucleus level RNA sequencing (RNA-seq) data to explore the relationship between expression of glycosylation-related genes (glycogenes) and N-glycosylation in the context of primate brain evolution. Last, by comprehensively characterizing the spatiotemporal dynamics of N-glycosylation during human brain development, we shed light on the neurodevelopmental trends that govern the maturation of the human brain N-glycome.

RESULTS

Overview of the Euarchontoglires brain N-glycome

Total N-glycans were isolated from brain tissue (table S1 and S2), labeled with 2-aminobenzamide (2-AB), and separated chromatographically as previously described (*14*), yielding a complex N-glycoprofile (Fig. 2A). MALDI-TOF/TOF-MS/MS analysis revealed 145 distinct monosaccharide compositions, which account for a total of 287 distinct N-glycan structures across all adult brain regions and species (table S3), including those with distinctive structural features typical of brain N-glycans (Supplementary Text and figs. S3 to S5). Notably, only 60 N-glycans (table S4) were ubiquitously present in all brain regions of all species, and their combined abundance disproportionately accounts for approximately 75% of the entire brain N-glycome. This conserved "core network" (Fig. 2B) predominantly consists of oligomannose and neutral fucosylated hybrid/complex structures, supporting the assertion that although there is a tremendous amount of structural diversity among brain N-glycans (*12*), a relatively small number of simple N-glycans comprise the bulk of the brain N-glycome (*15*).

For each group, we quantified the abundance of individual N-glycan peaks (figs. S6 and S7 and table S5 and S6) and, in turn, the resulting derived N-glycan traits (figs. S8 to S10 and table S7 and S8), which provided us with an overview of the composition of all the N-glycomes (fig. S11). It emerges that, quantitatively and qualitatively, the various brain N-glycoprofiles are generally similar and conform to the same overall "brain N-glycosylation template" characterized by an abundance of oligomannose (34 to 44%) and hybrid structures (6 to 12%), with the remainder being complex N-glycans (41 to 54%) along with a minor proportion of truncated (<6%) and paucimannose (<3%) N-glycans. Despite their overall similarity, careful examination of the differences between N-glycomes revealed a wealth of anatomical and phylogenetic variation in both the abundance and content of individual peaks (Supplementary Text, fig. S12, and table S5 and S6), which is ultimately reflected in statistically significant differences in derived N-glycan traits (table S8).

Distinctiveness of the cerebellar N-glycome

To explore the relationship between the various brain N-glycomes at a global level, we analyzed N-glycan peak abundance data using hierarchical clustering and *t*-distributed stochastic neighbor embedding (*t*-SNE). These analyses showed that the CBC exhibits the most distinctive N-glycome to the extent that it even overrides large phylogenetic distances (Fig. 3, A and B). This observation mirrors the results of similar analyses of the brain transcriptome and proteome (*16*, *17*) and suggests that the cerebellar N-glycome diverged from that of the remaining brain regions early and has remained well conserved throughout evolution. The defining feature of the cerebellar N-glycome is an increased abundance of the M6 N-glycan (Fig. 3C and figs. S6 and S10A). Nonetheless, phylogenetic divergence within the CBC cluster was also apparent and can be attributed to lineage-specific alterations in various N-glycan traits, including a human-specific increase in galactosylation density (Fig. 3, D and E). Subsequent clustering of brain N-glycomes was much more dependent on phylogeny than brain region, indicating that substantial interspecies variation in N-glycosylation is a feature of the remaining brain regions.

Intraspecies anatomical variation in brain N-glycosylation

Although the general features of brain-type N-glycosylation are conserved, the composition of the N-glycome varies across different brain regions (figs. S6, S8, and S10 to S12 and table S3). Generally, the same nominally significant anatomical trends were consistently observed in all species, although they more frequently survived correction for multiple testing in rats, likely because of their lower interindividual variability (fig. S1 and Supplementary Text). The most notable anatomical trend was a gradient of increasing complex N-glycan abundance from the CBC, through the STR, to the cortical structures (Supplementary Text and Fig. 4, A to D). This was accompanied by a complementary increase in features associated with complex N-glycans (e.g., galactosylation, fucosylation, and branching), which again is most evident in rats (fig. S8).

Because the hindbrain and the basal ganglia are overall more conserved across the analyzed species than the neocortex (*18*), this anatomical gradient of increasing N-glycome complexity appears to be inversely correlated to the degree of evolutionary conservation of the analyzed brain regions (Fig. 4E). Nevertheless, analysis of a broader range of diverse brain regions is needed to determine whether this pattern can be applied as a general rule throughout the brain, while studies of larger and more homogeneous primate cohorts are necessary to confirm whether these neuroanatomical patterns of N-glycosylation are evolutionarily conserved.

Phylogenetic trends and human-specific features of the brain N-glycome

Comparing the N-glycosylation profiles of equivalent homologous regions across species allowed us to gain insights into how the neuroglycome has changed over the course of Euarchontoglires evolution (Supplementary Text and figs. S9 and S10B). First, we observed a marked linear trend in the relative abundance of complex N-glycans, which, in all brain regions, was lowest in rats, slightly higher in macaques, and greatest in the hominid species (Fig. 5, A to D, and fig. S9). The rates of change were consistent with the evolutionary distance between species, indicating a gradual and uniform change over time (fig. S13). This phylogenetic gradient in brain N-glycome complexity parallels the gradient observed in a comparative brain lipidome study (*19*). Integrating information regarding the spatial and phylogenetic variation in complex N-glycan abundance, we found that peak N-glycome complexity occurs in the hominid cortical regions (Fig. 5H).

Second, we observed a notable phylogenetic trend toward increased usage of α(2-6)–linked Neu5Ac moving from rats, through macaques, to the hominids, which manifested as a decrease in the proportion of sialylated complex N-glycans homogeneously adorned with α(2-3)–linked Neu5Ac coupled with a corresponding increase in those carrying exclusively α(2-6)–linked Neu5Ac or those carrying both α(2-3)– and α(2-6)–linked Neu5Ac. The same overall trend was observed both at the whole brain level using aggregate data (Fig. 5, E to G) and when individual brain regions were analyzed separately (fig. S14). Comparing the linear regression results also offers some insight into the differing rates of evolutionary change for various brain N-glycosylation traits. Unlike the phylogenetic gradient in complex N-glycan abundance, the shifts in sialic acid linkage had relatively low correlation coefficients, indicating that these changes have been nonlinear over the evolutionary time scale in question. The spread of data points suggests an

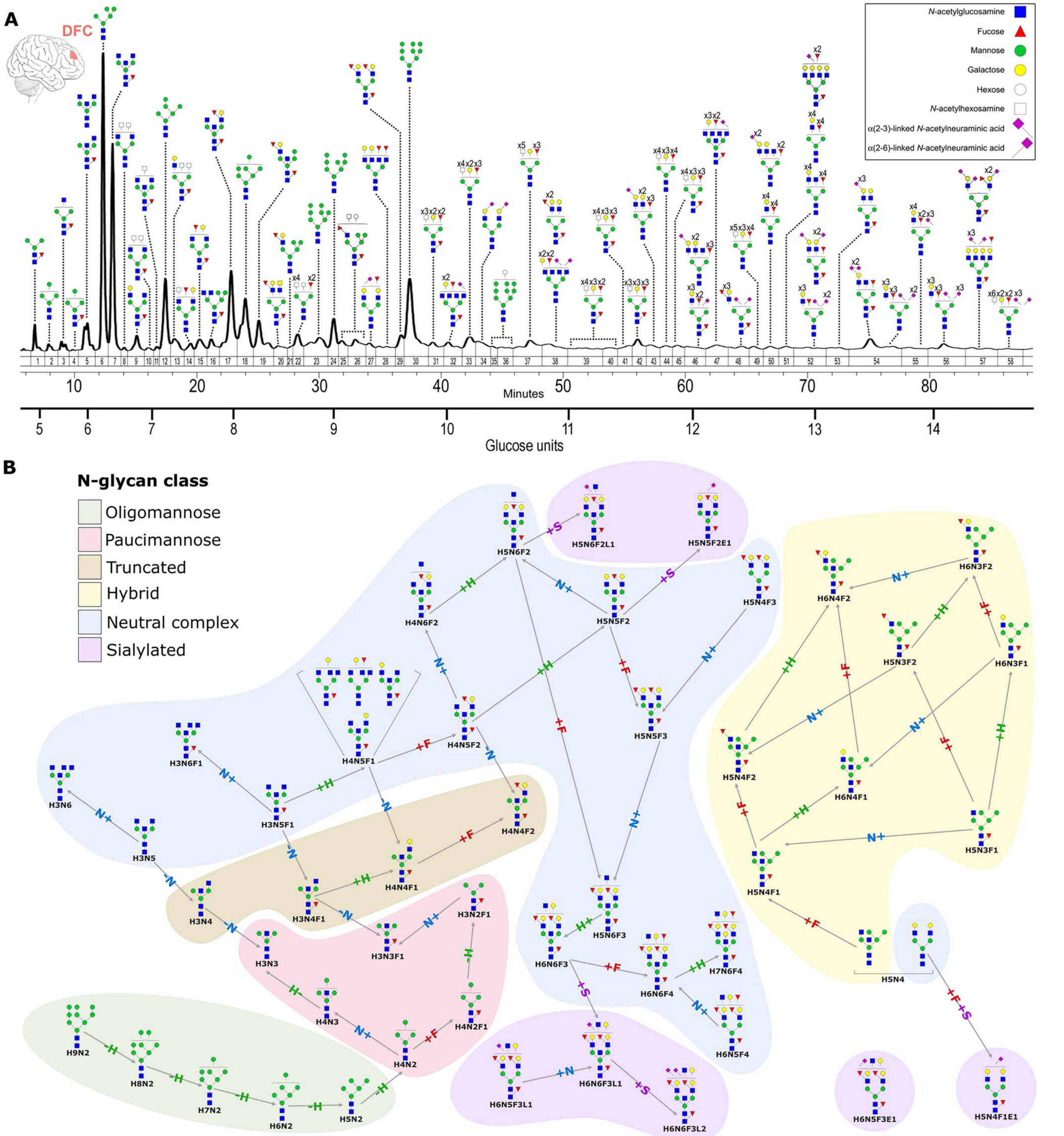

Fig. 2. Organization of the Euarchontoglires brain N-glycome. (**A**) Representative chromatogram of N-glycans derived from the human DFC annotated with proposed structures. Only the major N-glycan species in each peak are shown (see table S3 for complete list). Chromatographic peaks are labeled (1 to 58), and integration boundaries are shown as vertical lines. The *x* axis displays analyte retention time, while the *y* axis shows fluorescence at 428 nm. (**B**) Overview of the conserved brain N-glycome "core network" based on the 60 ubiquitous N-glycans that were detected in all brain regions of all species. The network was constructed using with the assumption that the core N-glycan structures are biosynthetically related. H, hexose; N, *N*-acetylhexosamine; F, deoxyhexose; L, α(2-3)–linked Neu5Ac (lactonized); E, α(2-6)–linked Neu5Ac (esterified).

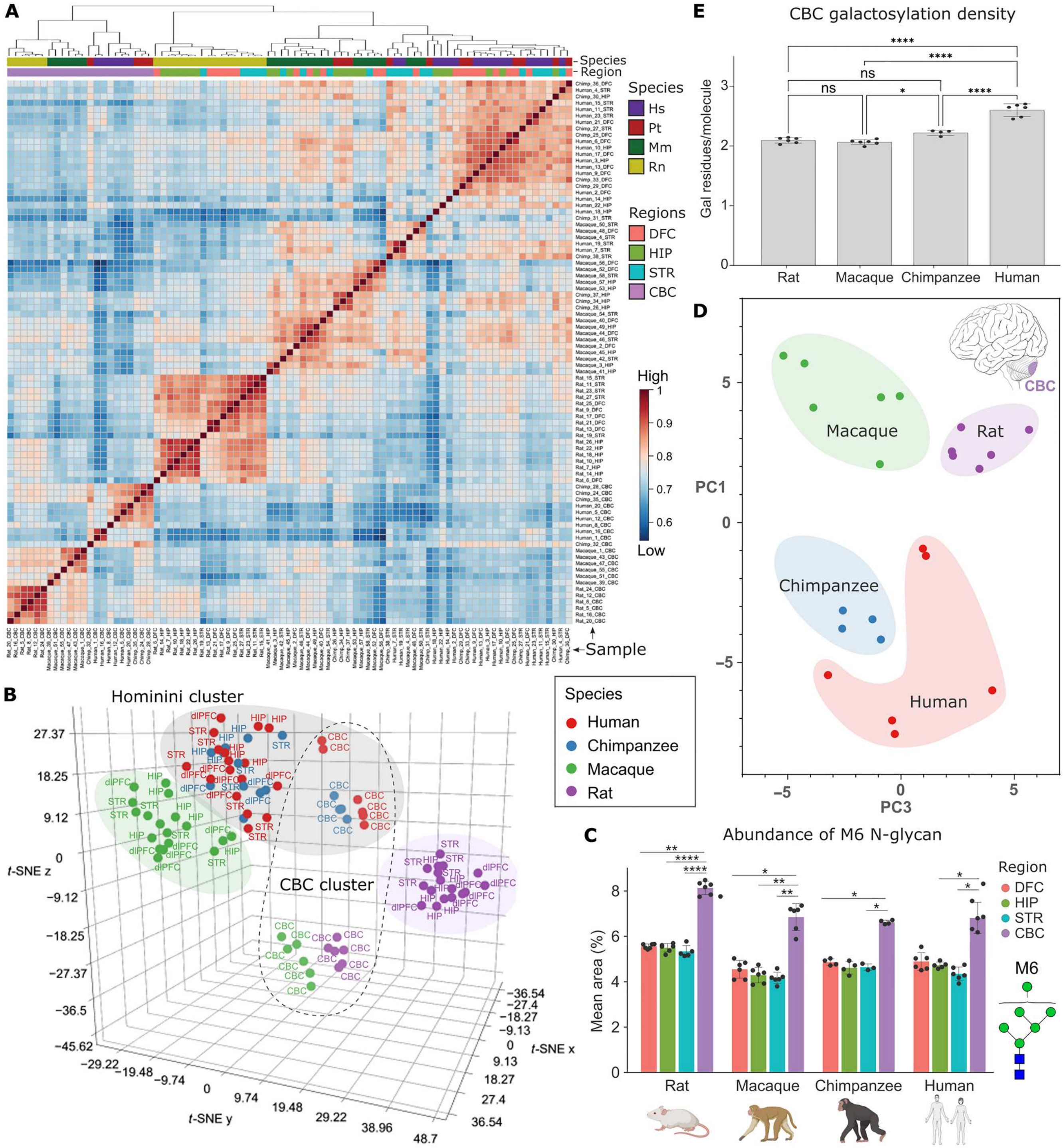

Fig. 3. The brain N-glycome is characterized by both anatomical and phylogenetic variation. (**A** and **B**) The relationships between the various mammalian brain N-glycomes were assessed using their UPLC-derived total N-glycoprofiles (i.e., the relative abundance of corresponding N-glycan peaks). (A) Kendall rank correlation heatmap and dendrograms illustrating the degree of correlation among the brain N-glycomes (color key indicates the strength of the correlation). (B) Three-dimensional *t*-SNE scatter plot illustrating the degree of relatedness between brain N-glycomes. Note that the CBC N-glycomes from all species form a distinct cluster separate from the other brain regions and that the hominini CBC N-glycomes are separated from those of macaques and rats. Axes represent the *t*-SNE *x*, *y*, and *z* dimensions. Species key for scatterplots is located at the center of the image. (**C**) In all species, the CBC N-glycome is characterized by an increased abundance of the M6 oligomannose N-glycan found in chromatographic peak 12. (**D** and **E**) Phylogenetic divergence of CBC N-glycomes. (D) PCA scatter plot of CBC N-glycomes. The *x* axis and *y* axis display the first (PC1) and third (PC3) principal components, respectively. (E) The human CBC has the highest galactosylation density (expressed as the mean number of galactose residues per galactosylated N-glycan) of all species. Statistical significance between groups was tested using ANCOVA (C) or one-way ANOVA (E) with correction for multiple testing using the Bonferroni procedure. Adjusted *P* values: *0.05 > *P* > 0.01; **0.01 > *P* > 0.001; and ****$P < 0.0001$; ns, not significant.

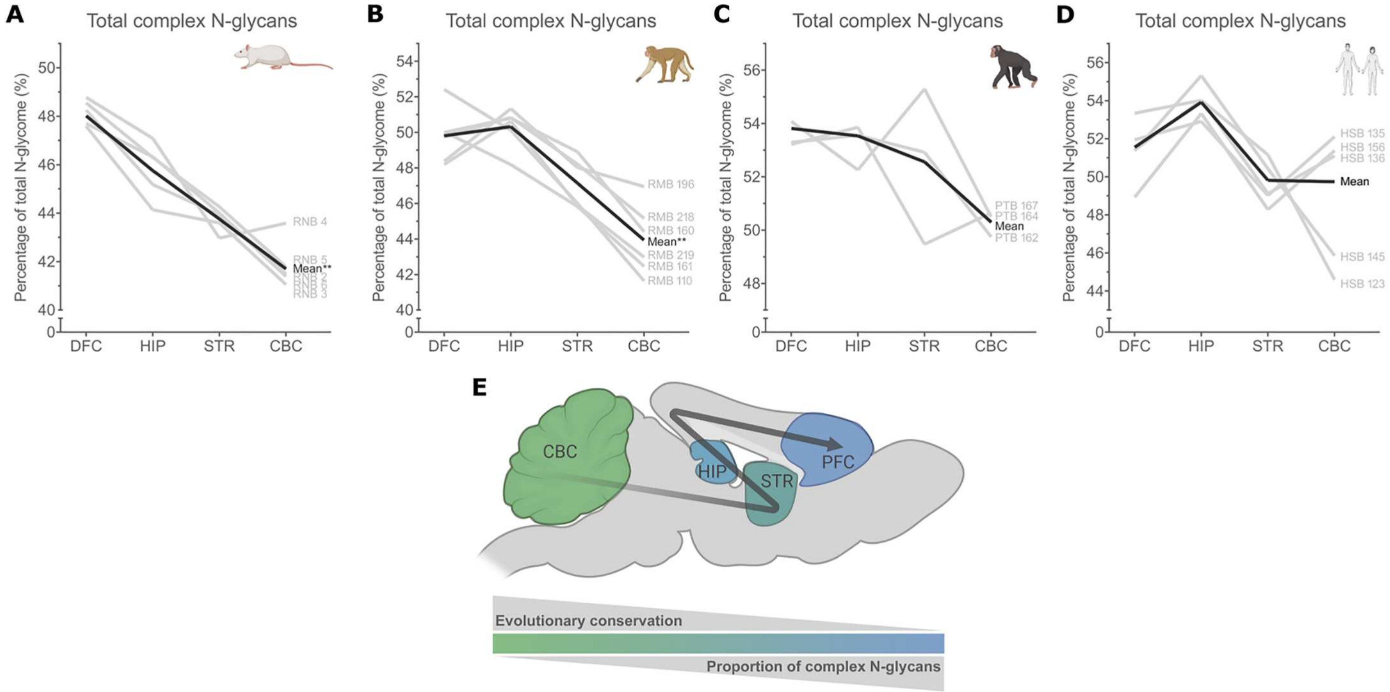

Fig. 4. Anatomical variation in complex N-glycan abundance in various Euarchontoglires brain N-glycomes. Total complex N-glycan content in the (**A**) rat, (**B**) macaque, (**C**) chimpanzee, and (**D**) human brain N-glycome according to brain region. Gray lines show complex N-glycan content across different brain regions of individual animals or donors (labels shown on the right). The black line shows the group mean. Only subjects with data for all brain regions are plotted. Data were analyzed using mixed model analysis, and a test for linear trend across brain regions (in the order shown from left to right) was performed with correction for multiple testing using the Bonferroni procedure. Adjusted *P* values: $^{**}P < 0.01$. (**E**) Schematic illustrating the proposed anatomical gradient in Euarchontoglires brain N-glycome complexity. A rat brain is shown for illustrative purposes, although a similar and nominally significant trend was observed in all species examined, indicating that this may be a conserved feature. Our data suggest that there is general trend toward increasing abundance of complex N-glycans from the CBC, through the STR, to the cortical structures, which is accompanied by a corresponding decrease in the proportion of noncomplex (i.e., oligomannose, paucimannose, hybrid, and truncated) N-glycans. This gradient inversely correlates to the pattern of evolutionary conservation of brain regions in vertebrates, which suggests that highly conserved brain regions have a higher proportion of ancient, minimally processed N-glycans, while less conserved brain regions have acquired N-glycoprofiles of greater complexity. DFC, dorsolateral prefrontal cortex; PFC, prefrontal cortex; HIP, hippocampus; STR, striatum; CBC, cerebellar cortex.

accelerated rate of change for this trait during primate evolution, particularly in the human lineage.

Detailed analysis of both Neu5Ac density and linkage among sialylated complex N-glycans revealed that the most notable difference occurs in disialylated N-glycans homogeneously adorned with α(2-6)–linked Neu5Ac, which are considerably more prevalent in human brains, particularly in the forebrain regions where such structures are virtually absent in other species (with the exception of the macaque STR; fig. S15). It also uncovered a notable Neu5Ac usage pattern specific to primates. Namely, although tetrasialylated L1E3 variants [i.e., carrying one lactonized α(2-3)–linked Neu5Ac residue (L1) and three esterified α(2-6)–linked Neu5Ac residues (E3)] were relatively abundant in primate forebrain regions, these variants were detected only as minor structures in rat brains. Overall, our data indicate that the evolution of the human brain N-glycome was characterized by a brain-wide increase in N-glycome complexity coupled with a shift toward greater usage of α(2-6)–linked Neu5Ac (Fig. 5I).

In addition to these broad evolutionary trends, we also observed clear taxon-specific differences in brain N-glycosylation (Supplementary Text and figs. S9 and S10B; summarized in Fig. 6), including several human-specific features of the brain N-glycome that were predominantly related to differences in Neu5Ac linkage.

Rapid divergence of primate brain N-glycomes

We next investigated the relationship between glycogene expression and N-glycosylation in primate brains by integrating our N-glycomics data with complementary bulk RNA-seq data (*17*). To narrow our focus to biologically relevant genes, we compiled a list of 47 glycogenes encoding enzymes that are predominantly involved in N-glycan synthesis (table S9). Clustering the primate glycogene expression profiles according to overall similarity, we observed that, as was the case with the N-glycome, the CBC had the most distinct expression profile which overrides species differences (fig. S16). However, unlike the N-glycome, subsequent clustering was much more dependent on brain region than species, indicating that, in the brain, interspecies differences in glycogene expression are less pronounced than interspecies differences in N-glycosylation.

We further explored the extent to which glycogene expression in the brain is conserved among primates using Mantel correlograms to assess the interspecies correlation between each primate pair for the entire set of 47 glycogenes (Fig. 7A). This resulted in strong correlations, indicating that glycogene expression in primate brains is very highly conserved compared to nonglycogenes (fig. S17). These data are consistent with evidence demonstrating that glycogenes involved in N-glycosylation are highly conserved at the sequence level across primates (*20*) and further support the notion that the

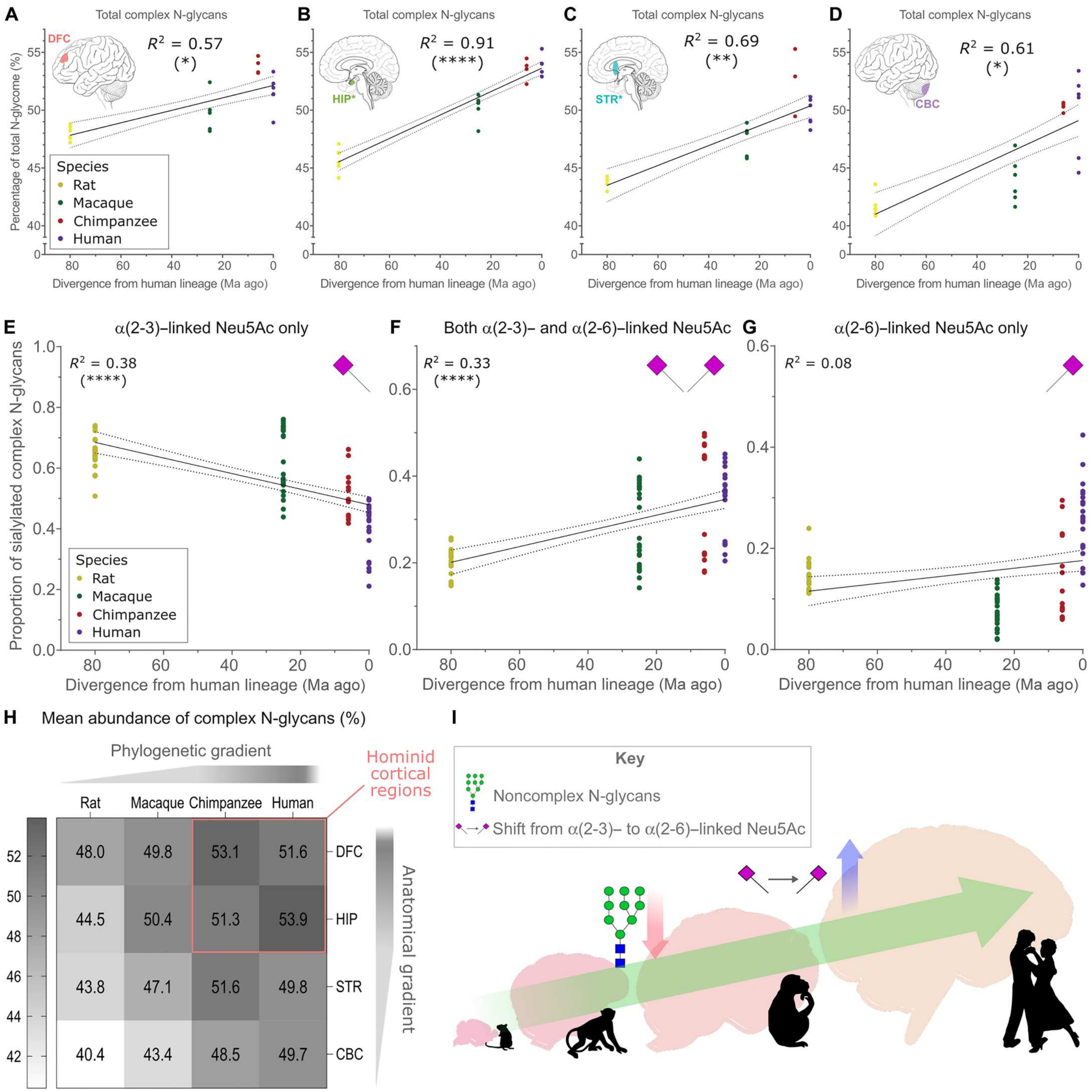

Fig. 5. Phylogenetic trends in Euarchontoglires brain N-glycosylation. Phylogenetic gradient of complex N-glycan abundance in the (**A**) DFC, (**B**) HIP, (**C**) STR, and (**D**) CBC. Data were analyzed using linear regression (90% confidence intervals and R^2 values are shown). Asterisks in parentheses indicate lines whose slopes were significantly nonzero after correction for multiple testing using the Bonferroni procedure. Adjusted P values: $^{*}0.05 > P \geq 0.01$, $^{**}0.01 > P \geq 0.001$, and $^{****}P < 0.0001$. Ma, million years. (**E** to **G**) Phylogenetic trends in Neu5Ac linkage distribution. The plots show the proportion of sialylated complex N-glycans carrying only α(2-3)–linked Neu5Ac (E), both α(2-3)– and α(2-6)–linked Neu5Ac (F), or only α(2-6)–linked Neu5Ac (G). Aggregate (i.e., whole brain) data are plotted and were analyzed as in (A to D). See fig. S14 for individual brain region data. (**H**) Heatmap of mean complex N-glycan abundance (expressed as a percentage of total N-glycome) for each brain N-glycome. As a result of overlapping anatomical (see Fig. 4) and phylogenetic gradients in the abundance of complex N-glycans, peak N-glycome complexity occurs in the hominid cortical regions. (**I**) Schematic illustrating the proposed evolutionary trends that have shaped the human brain N-glycome. Our data indicate that the evolution of the human brain N-glycome has been marked by a global increase in complexity and a shift toward greater usage of α(2-6)–linked Neu5Ac.

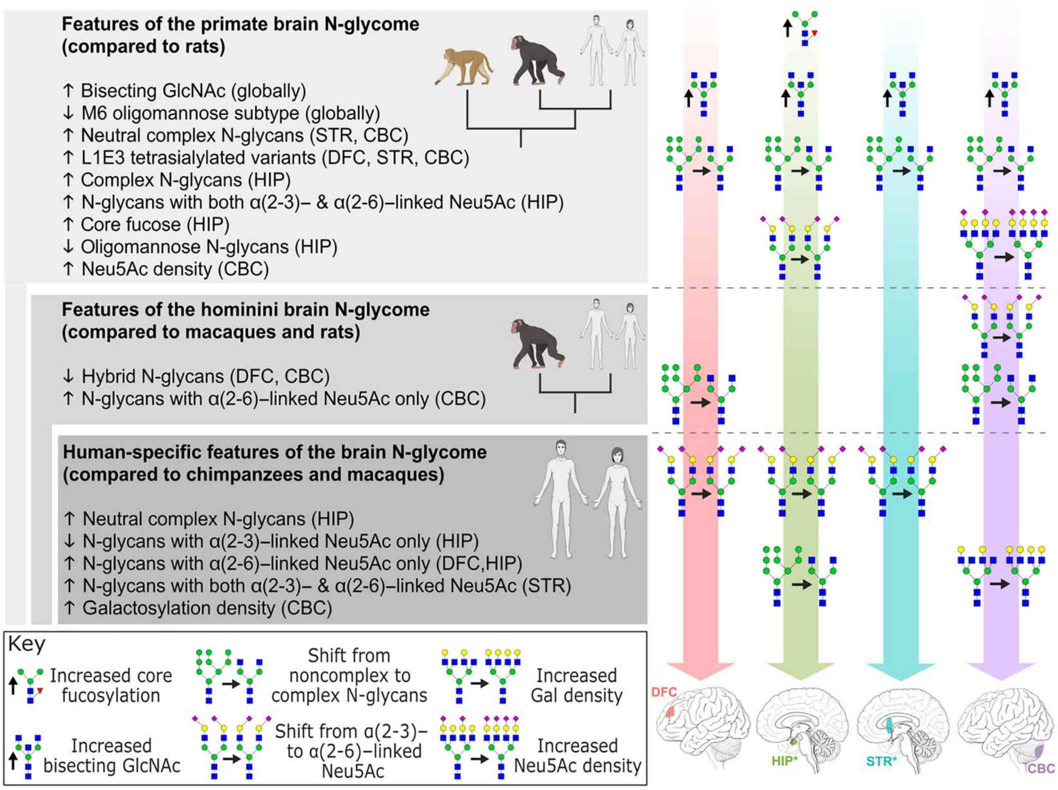

Fig. 6. Summary of statistically significant taxon-specific differences in N-glycosylation for each brain region. For clarity, traits that result in an increase in the proportion of complex N-glycans have been symbolically grouped together, as have those that result in an increase in the proportion of α(2-6)–linked Neu5Ac. *Denotes that regions are internal and not visible from the view shown. See Supplementary Text and table S8 for details. DFC, dorsolateral prefrontal cortex; HIP, hippocampus; STR, striatum; CBC, cerebellar cortex.

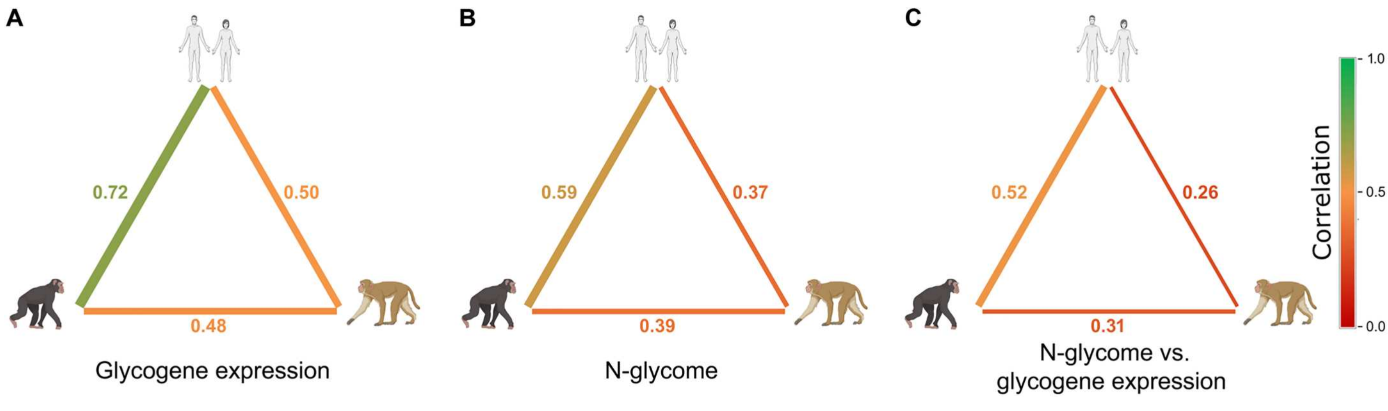

Fig. 7. The N-glycomes of primate brains are less conserved than the expression of the underlying glycogenes. The correlation between each primate pair was determined with regard to (**A**) glycogene expression, (**B**) the N-glycome, and (**C**) the correlation between glycogene expression and the N-glycome phenotype. A Mantel test was used for (A) and (B), while the correlation of Pearson coefficients was used for (C). The thickness and color of the lines connecting species indicate the strength of the correlation (thicker lines represent stronger correlations).

products of these genes operate in a highly constrained functional network. Repeating the procedure for the primate brain N-glycome profiles resulted in weaker correlations (Fig. 7B), indicating that N-glycosylation of brain proteins is generally less conserved than the expression of the associated glycosylation enzymes. Next, Pearson correlation coefficients were calculated to determine the linear correlation between glycogene expression and the N-glycome in each primate species. Interspecies correlation of these coefficients produced weaker correlations still (Fig. 7C), indicating poor conservation of the relationship between these two traits across evolution. These findings are consistent with other studies that have shown that the relationship between glycogene expression and the final glycosylation phenotype is complex and that changes in gene expression do not always correlate with the predicted changes in cell surface glycan expression (*21*). This is likely due to the multilevel regulation of protein glycosylation and may be compounded by the generally low abundance of glycosyltransferases (*22*, *23*). Last, we demonstrate that although the correlation between glycogene expression and N-glycosylation phenotype in primate brains is generally weak (fig. S18A), it is nevertheless possible to uncover putative associations between N-glycan structures and the expression of specific glycogenes using a bioinformatics prioritization strategy (Supplementary Text and fig. S18). Overall, our observations of accelerated evolutionary divergence at the N-glycome level are consistent with examples of interspecies glycan diversity at the level of orthologous glycoproteins (*24*) and support the notion that divergent posttranslational modification of conserved proteins via N-glycosylation is a means of generating additional diversity among closely related organisms.

Regional and cell type profiling of glycogene expression in primate brains

We compared glycogene expression across human brain regions and observed that the majority of glycogenes (29 of 47) could be classified into one of a handful of recurring expression profiles exhibiting clear regional specificity (Fig. 8A). Of these, almost half showed either enriched or depleted expression specifically in the CBC. We validated the expression of a selection of glycogenes using digital droplet polymerase chain reaction (ddPCR; fig. S19). In keeping with the clustering data, the spatial expression patterns of glycogenes are mostly conserved among primates (fig. S20), although there were some notable exceptions. We identified four glycogenes exhibiting human-specific spatial mRNA expression profiles in at least one brain region: *B3GALT5*, *ST3GAL2*, *ST6GAL2*, and *ST8SIA6* (fig. S21). ST3GAL2 expression in the primate brain was further investigated at the protein level using immunohistochemistry (fig. S22). These results not only partially validated the bulk RNA-seq expression data by confirming human-specific down-regulation of ST3GAL2 in the prefrontal cortex but also revealed further differences that were not detected in the bulk tissue analysis. Namely, Purkinje cells of the human CBC ubiquitously express ST3GAL2, while the proportion of ST3GAL2-expressing Purkinje cells is significantly lower in chimpanzees (approximately 70%) and macaques (0%). Nevertheless, although ST3GAL2 is not expressed in macaque Purkinje cells, we found that it is more highly expressed in granule cells and cells of the molecular layer in macaques than in the other primates. These results indicate that some of the phylogenetic divergence in gene expression likely arises from interspecies differences at the cell type level rather than simple up- or down-regulation (i.e., molecules/cell) within the same cell types and thus highlight the limitations of bulk tissue analysis, as well as the need for validation using orthogonal methods that have single-cell resolution and/or histological context (Supplementary Text).

Next, we made use of primate DFC single-nucleus RNA-seq (snRNA-seq) expression data (*25*) to characterize glycogene expression across neural cell types. Clustering the glycogenes according to their expression profile revealed distinct heterogeneity in their cell type distribution (Fig. 8B and fig. S23). Generally, neurons have a broader palette of glycogene expression than non-neuronal cell types because expression of glycogenes from clusters 3 to 5 is largely absent from the latter. There were few differences in glycogene expression between excitatory and inhibitory neurons. Although the overall clustering pattern was largely conserved in primates, some evolutionary divergence was evident (Fig. 8, B and C). In particular, our data show that the vast majority of differences in glycogene expression between macaques and hominids occurred in non-neuronal cell types in which glycogene expression has been extensively repressed in the hominid lineage. The expression of three sialyltransferases involved in the addition of α(2-6)–linked Neu5Ac to glycoconjugates (*ST6GAL1*, *ST6GALNAC3*, and *ST6GALNAC5*) was notably enriched in the human lineage across several cell types, which may be one of the factors contributing to the increased abundance of α(2-6)–linked Neu5Ac in humans (Fig. 5).

To investigate whether the differences in brain N-glycosylation that we observed between primate species arise because of differences in the expression of glycosylation enzymes (glycoenzymes), we investigated the expression of proteins encoded by glycogenes in the DFC of the three primate species using a liquid chromatography with tandem mass spectrometry (LC-MS/MS) proteomics approach. However, we were only able to detect the expression of four of the 47 glycoenzymes selected for analysis (table S10), namely, HEXA, HEXB, MAN2C1, and FUT9 (Supplementary Text and fig. S24). This detection rate (9%) was four times lower than for randomly chosen control proteins (169 detected from 470 selected, i.e., 36%), indicating that, although our method generally works well for most proteins, glycoenzymes are expressed at much lower levels than other types of proteins. This is consistent with reports by others stating that glycogenes are generally expressed at very low abundance (*22*) and have exceptionally low translation efficiency (*23*). Thus, because of a combination of the technical limitations of this method and the inherently low abundance of glycoenzymes, our ability to correlate our N-glycomics results to phylogenetic differences in the expression of glycoenzymes was limited.

Spatial diversification of the human brain N-glycome during neurodevelopment

Next, we investigated the developmental pathways that shape the adult brain N-glycome by analyzing the corresponding brain regions in the prenatal human brain using a similar multi-omics approach. We show that the mid-fetal brain has already acquired the archetypal "brain-type" N-glycosylation profile by postconception week (PCW) 21 (fig. S25). This early specification of the brain N-glycome is also evident at an equivalent stage (*26*) of neurodevelopment (i.e., postnatal day 0) in rats (*27*), suggesting that it may be a conserved feature in mammals, although investigation of earlier time points will be required to determine the precise stage of neurodevelopment at which the archetypal brain N-glycome first emerges. Despite the overall similarity between the prenatal and adult brain N-glycomes (fig. S25 to S29 and table S11), specific qualitative differences were observed at the level of individual chromatographic peaks that were either widespread (fig. S30) or region-specific (fig. S31 to S33) and ultimately reflected developmental differences in the global composition of the N-glycome (fig. S34). We also identified numerous N-glycan peaks and structures that were enriched in either the fetal or the adult brain (Supplementary Text and figs. S35 to S38). Hierarchical clustering and principal components analysis (PCA) of the global N-glycome showed that N-glycosylation in the mid-fetal brain is regionally more homogeneous than in the adult brain and, moreover, that the CBC N-glycome has not yet become differentiated (Fig. 9, A and B). This

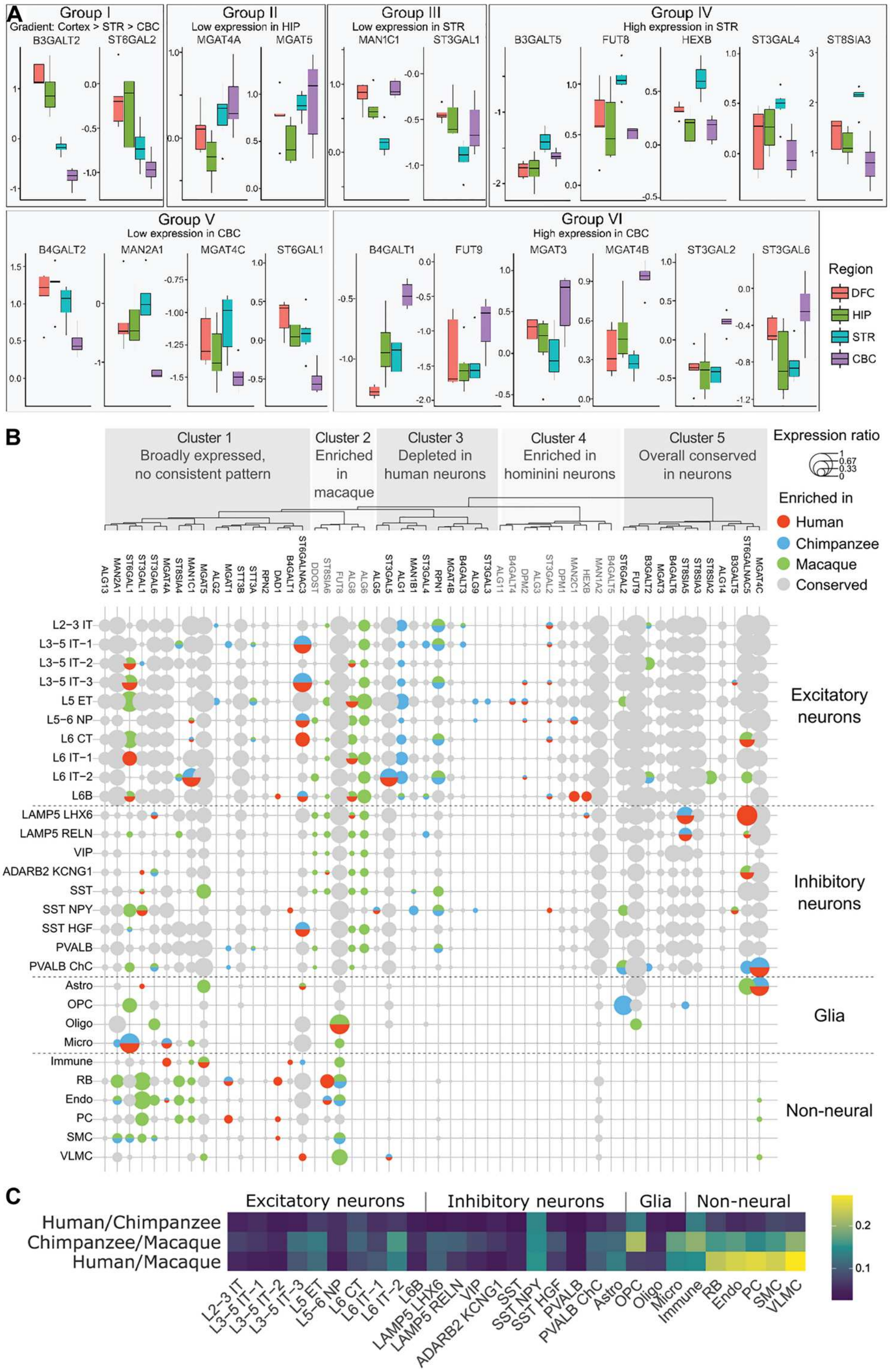

Fig. 8. Human-specific and cell type–specific expression patterns of particular glycogenes. (**A**) Examples showing the categorization of glycogenes according to shared spatial expression profiles in human brains. The *y* axes show scaled expression of logRPKM values within samples and among the 47 glycogenes. (**B**) Cell type distribution of glycogene expression in the adult primate DFC. The dot color represents species expression enrichment or conservation (gray). The dot size indicates the average expression ratio in the enriched species (species-specific expression) or all the species (conserved expression). The dendrogram shows clustering of glycogenes according to their pattern of cell type expression across species. (**C**) Phylogenetic divergence of glycogene expression in the primate DFC across various cell types. Here, the dissimilarity in aggregate glycogene expression between pairs of primate species in each cell cluster was measured as the Pearson correlation coefficients of the average expression subtracted from 1 and is shown as a heatmap. Cell type abbreviations: L, layer; IT, intratelencephalic neurons; ET, extratelencephalic neurons; NP, near-projecting; CT, cortical-thalamic projection neurons; ChC, chandelier cells; Astro, astrocytes; OPC, oligodendrocyte precursor cells; Oligo, oligodendrocytes; Micro, microglia; Immune, immune cells; RB, red blood lineage cells; Endo, endothelial cells; SMC, smooth muscle cells; VLMC, vascular leptomeningeal cells.

observation contrasts with findings in which regional differences in gene expression were more pronounced during prenatal development than in adulthood (*28*). This may indicate that the more diverse N-glycome of the adult brain compensates for the restricted spatial diversity of the transcriptome and provides an additional layer of regional differentiation. When examining only sialylation features, we observed further regional differentiation in the adult brain with the HIP diverging from the other forebrain regions (Fig. 6C). We identified four N-glycan clusters whose abundance was differentially regulated throughout neurodevelopment, particularly in the CBC (Fig. 9A). Together, our data suggest that region-specific N-glycosylation programs lead to greater diversification of the human brain N-glycome throughout neurodevelopment,

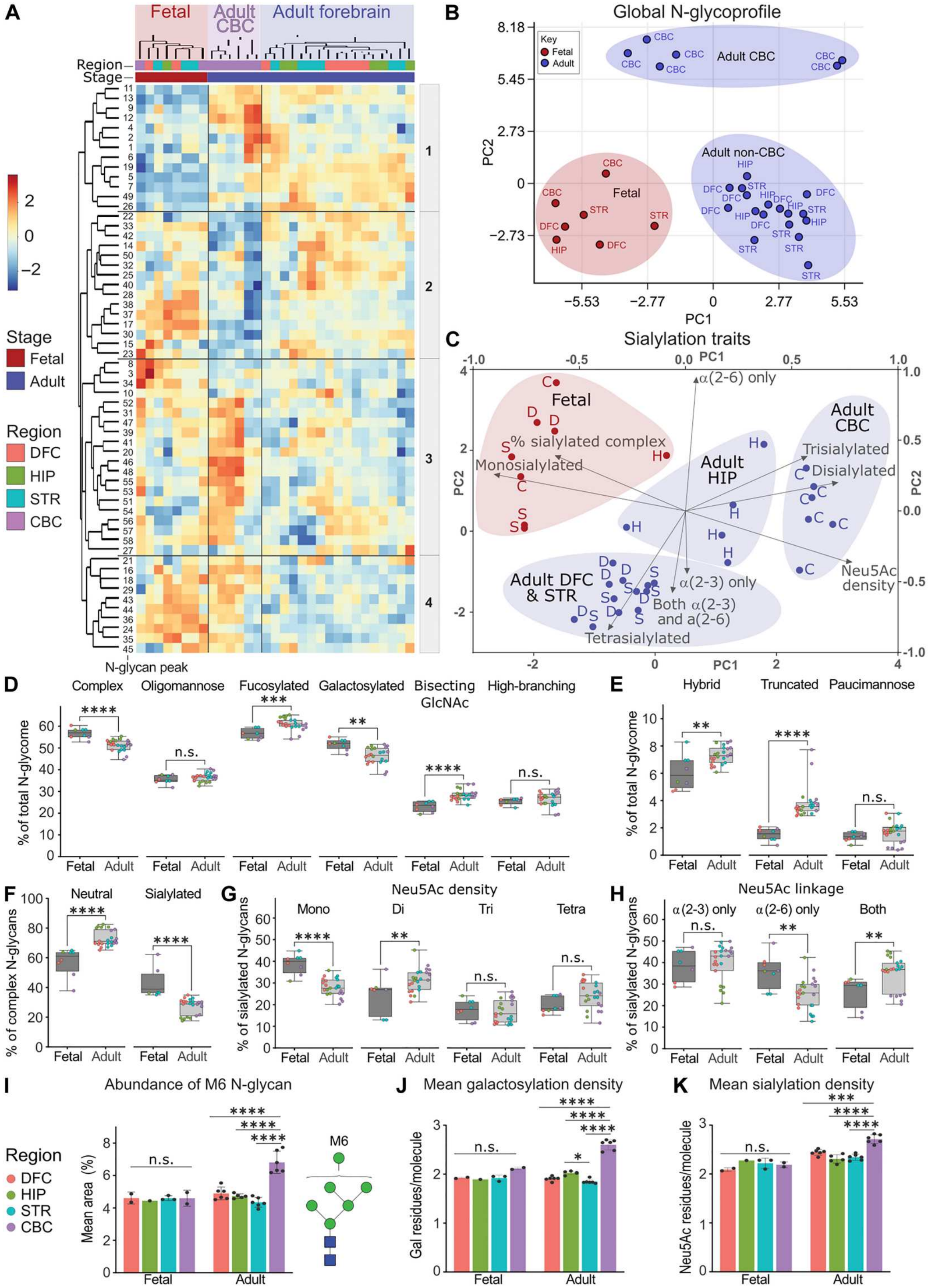

Fig. 9. Global and region-specific maturation pathways lead to distinct spatial N-glycosylation profiles in the adult human brain. (**A**) Hierarchical clustering of quantitative UPLC N-glycan peak abundance. The heatmap shows the relative abundance of each chromatographic peak across samples. Developmentally regulated N-glycan peak clusters are indicated (1 to 4). (**B** and **C**) Scatter plots illustrating the degree of relatedness among the human brain N-glycomes throughout ontogeny according to the total global N-glycome (B) or sialylation features only (C). The axes display the first (PC1) and second (PC2) principal components. In (C), the left and bottom axes refer to the loadings, while the top and right axes refer to the scatter plot. D, dorsolateral prefrontal cortex; H, hippocampus; S, striatum; C, cerebellar cortex. (**D** to **H**) Global developmental trends in brain N-glycosylation. Aggregate data for the indicated derived traits were analyzed using unpaired, two-tailed *t* tests. Box and whisker plots show the data spread including the median value, interquartile range, maximum, and minimum. Data points are colored by brain region [key in (I)]. (**I** to **K**) CBC-specific features of N-glycome maturation. Data for the indicated derived traits were analyzed using ANOVA with correction for multiple testing using the Bonferroni procedure. Adjusted *P* values: ****0.0001 > *P*, ***0.001 > *P* > 0.0001, **0.01 > *P* > 0.001, and *0.05 > *P* > 0.01.

particularly in the CBC, which acquires a distinctive N-glycome between the late mid-fetal stage and adulthood.

Global maturation of the brain N-glycome, which proceeds similarly in all regions (fig. S39), is characterized by an increase in the proportion of hybrid and truncated N-glycans at the expense of complex types, predominantly those that are sialylated (Fig. 9, D to F, and fig. S40). The proportion of oligomannose N-glycans remained relatively stable across development throughout all brain regions (Fig. 9D), although we observed a slight redistribution of the major oligomannose subtypes with the profile being skewed toward smaller subtypes in adults, mainly at the expense of the M9 form (fig. S41). These findings are consistent with results from rodent studies (*27*, *29*, *30*), although the shift in subtype usage seen in the human brain is not as marked. Notably, at 21 PCW, the fetal CBC does not yet exhibit elevated levels of the M6 subtype (Fig. 9I). Regarding structural features, the proportion of N-glycans modified by either sialylation or galactosylation decreases as neurodevelopment proceeds, while the prevalence of fucosylated structures and those with bisecting *N*-acetylglucosamine (GlcNAc) increases (Fig. 9D). We also observed changes in the density of such modifications (Supplementary Text and fig. S42). CBC-specific maturation of the N-glycome was characterized by an increase in the abundance of the M6 structure along with increases in both galactosylation and sialylation density (Fig. 9, I to K).

Last, our data indicate that the human brain N-glycome undergoes extensive changes in the regulation of N-glycan sialylation during neurodevelopment (Fig. 9, G and H; Supplementary Text; and figs. S43 and S44). Briefly, we found that a smaller proportion of N-glycan structures are sialylated in the mature brain than the developing brain, although the ones that are sialylated tend to carry a greater number of Neu5Ac residues and, moreover, there is a trend toward increased usage of α(2-3)–linked Neu5Ac, which is most prominent in the DFC and STR. Similar developmental trends were observed in the mouse cerebral cortex (*31*), indicating that these may be conserved features of mammalian N-glycome maturation.

Spatiotemporally regulated glycogene expression in the human brain

Integration of our developmental N-glycomics data with complementary bulk RNA-seq transcriptomic data enabled us to identify numerous developmentally regulated glycogenes that showed either global or region-specific temporal dynamics (Supplementary Text and fig. S45), a selection of which were validated using ddPCR (fig. S46). Generally, their expression profiles closely matched the developmental trajectory of orthologous genes in the mouse cerebral cortex (*30*), indicating that the developmental regulation of specific glycogenes in the brain is well conserved in Euarchontoglires. In accordance with the CBC's distinctive N-glycome in the adult brain, the prevalence of region-specific developmental regulation of glycogene expression was highest in this brain region (Supplementary Text).

Last, we searched for associations between developmental changes in glycogene expression and the abundance of specific N-glycan peaks in corresponding brain regions to uncover potential causal relationships between the two variables using a bioinformatics prioritization strategy (Supplementary Text and fig. S47). Our analysis shows that, in certain instances, the differential expression of individual glycogenes can be linked to tangible and glycobiologically plausible changes in the N-glycome phenotype in a complex in vivo biological system, a finding that complements the work of others (*15*).

DISCUSSION

Our analysis revealed a wealth of anatomical, phylogenetic, and ontological variation in brain N-glycosylation patterns of Euarchontoglires mammals within the overall framework of a conserved template. Some of the most notable trends were related to changes in the relative abundance of complex versus noncomplex N-glycans. Evidence suggests that it is the latter, and particularly the ancient oligomannose class of N-glycans (*32*), that are essential for normal neuronal functioning, while complex N-glycans are dispensable (*33*). Rationally, it follows that high oligomannose content is a conserved feature of the brain N-glycome: one that many CNS pathogens have evolved to exploit (*34*). In contrast, complex N-glycans in the CNS appear to be under fewer evolutionary constraints, thus rendering them susceptible to progressive tinkering (e.g., switching Neu5Ac linkage), which can lead to innovation in certain phylogenetic lineages. As a result of overlapping anatomical and phylogenetic gradients in the abundance of complex N-glycans, peak N-glycome complexity was found in the hominid cortical regions, leading us to hypothesize that this increased diversity and complexity of sugar modifications found on neural N-glycoproteins contributed to the emergence of novel cognitive functions, including those unique to the human neocortex (*35*–*37*).

Numerous multiregional N-glycomics studies in various vertebrate species have shown that anatomical variation in N-glycosylation, although subtle, does exist between brain regions (*13*, *15*, *38*–*44*). In their investigation of N-glycosylation in the mouse brain, Williams and colleagues (*15*) also reported that the CBC is the region exhibiting the most distinctive N-glycome, although, in contrast to our findings, they concluded that the CBC has the highest abundance of complex N-glycans. Nevertheless, our results align with data from other studies in mouse (*41*) and zebrafish (*42*), demonstrating that the CBC has the highest abundance of oligomannose N-glycans, while the forebrain regions have a greater abundance of highly processed (i.e., galactosylated and fucosylated) N-glycans (*41*). Our work extends these findings to primates, indicating that spatial distribution of brain N-glycome complexity is generally well conserved in vertebrates.

One of the most notable evolutionary trends in N-glycosylation of brain proteins concerned the shift toward increasing usage of α(2-6)–linked Neu5Ac in humans. It is known that human evolution has been marked by numerous lineage-specific adaptations in sialic acid biology, including the complete loss of the ability to synthesize glycans containing *N*-glycolylneuraminic acid (Neu5Gc), changes in the ratio of sialic acid linkages in various tissues, and multiple changes in the structure and expression of Sia-recognizing immunoglobulin-like lectins (*45*). The available evidence suggests that the capping of glycans with sialic acids is one aspect of human physiology that is particularly susceptible to evolutionary change and, furthermore, that this can sometimes occur over a relatively short time scale.

An earlier comparative study of several hominid species identified human-specific regulation of sialic acid linkage in various tissues using lectin histochemistry (*46*). The authors stained fixed tissue sections with two lectins, *Maackia amurensis–II* (MAH) and *Sambucus nigra–I* (SNA), which preferentially bind α(2-3)– and α(2-6)–linked sialic acid, respectively, and reported that, in comparison to the other hominids, humans displayed higher expression of α(2-6)–linked sialic acid in some tissues (e.g., airway epithelial cells, eccrine sweat glands, and erythrocytes) but lower expression in others (e.g., appendix, ileal smooth muscle, liver bile ducts, ovary, skin, splenic cords, testes, and tonsils). They proposed that the human-specific shift toward α(2-6)–linked sialic acid in externally exposed tissues, which are the first point of contact for pathogens, were driven by interactions with Neu5Ac-binding pathogens, such as the animal influenza virus, which has a preference for the α(2-3)–linked form.

In their comprehensive study, Gagneux and colleagues also noted some differential lectin reactivity in the brain, most notably in the white matter; in orangutans the white matter was reactive only to MAH, in chimpanzees it was reactive to both MAH and SNA, while in humans it was reactive only to SNA. This interesting pattern could perhaps be interpreted as evidence that a gradual shift toward increased α(2-6)–linkage occurred in white matter in the human lineage (with chimpanzees representing an intermediate step in this process), and it broadly aligns with our results. However, it is difficult to directly compare results from our highly specific N-glycomics analysis with those from the mentioned study because of the vast differences in experimental methodology, the primary one being the lack of specificity and promiscuous affinity of lectins, which are known to bind multiple carbohydrate epitopes on various types of glycans (i.e., not only N-glycans) (*47*). Nevertheless, these observations have implications for our results and raise the possibility that the interspecies differences in α(2-6)–linked Neu5Ac that we report could be due to differences in white matter content that arise during tissue sampling or dissection. However, we rule this out because (i) no white matter was included in the hippocampal dissections and the trend was also observed in this brain region (fig. S14F), and (ii) great care was taken to perform all dissections as similarly as possible across all species, including with respect to the white matter content.

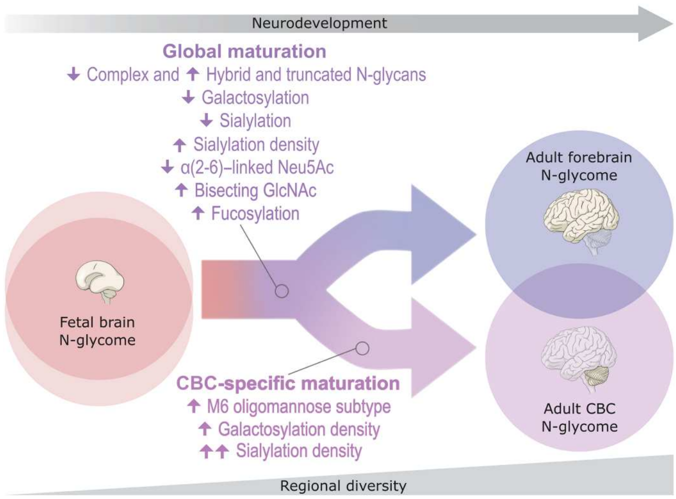

Fig. 10. Proposed model of the compositional transfiguration of the human brain N-glycome during neurodevelopment. As brain development proceeds, the fetal brain N-glycome, which is relatively homogeneous at 21 PCW, becomes more diversified via the combinatorial regulation of discrete N-glycan clusters eventually leading to divergent, but overlapping, region-specific N-glycosylation profiles in the adult brain and, consequently, greater regional diversity. General maturation of the brain N-glycome, which is common to all brain regions (including the CBC), is primarily characterized by a decrease in the proportion of complex N-glycans, a decrease in the proportion of sialylated and galactosylated N-glycans, and an increase in the prevalence of bisecting GlcNAc. In addition, complex sialylated N-glycans of the mature brain exhibit a greater density of Neu5Ac residues, and this is coupled with decreased usage of α(2-6)–linked Neu5Ac. The N-glycome of the adult CBC differs from those of the forebrain regions (DFC, HIP, and STR), suggesting that its maturation follows a distinct course. CBC-specific maturation is largely characterized by an increased prevalence of the M6 oligomannose subtype, as well as increased galactosylation and sialylation density.

Our transcriptomic data suggest that phylogenetic differences in the expression of α(2-6)–sialyltransferases may underpin the observed evolutionary shift in Neu5Ac linkage. Although analysis of various human tissues has shown that expression of the *ST6GAL2* transcript is enriched in the brain (*48*), its cell type expression profile was well conserved across the primate species (Fig. 8B), making it unlikely to be the key driver. Rather, we hypothesize that *ST6GAL1*, *ST6GALNAC3*, and *ST6GALNAC5* are good candidates, given their enriched expression in various cell types in humans (Fig. 8B). Ultimately, while the biological significance of this shift in Neu5Ac linkage in the brain is still unclear, given that the influenza virus can invade the CNS (*49*), we speculate that brain cells may also have been under strong selective pressure to switch their Neu5Ac linkage.

Our data show that, in comparison to glycogene expression networks, the brain N-glycome evolves rapidly and, given our results, we propose that the evolution of the brain N-glycome has been shaped by two opposing forces. On the one hand, an increase in the proportion of complex N-glycans would increase diversity and hence provide more scope for the development of novel functions while also enabling the host to evade pathogens that have evolved to exploit the brain's high oligomannose content. However, reducing oligomannose content too much may compromise essential neurobiological processes (*33*), which would negatively affect fitness. In such a trade-off, a delicate balance needs to be maintained, which may explain why the evolution of the brain N-glycome has been so incremental and, consequently, why the archetypal brain N-glycoprofile is so well conserved. Nevertheless, our data suggest that discrete brain N-glycosylation traits may be subject to differing rates of evolutionary change and that the human brain N-glycome has been shaped by both gradual changes occurring over a long evolutionary time scale, as well as relatively rapid changes in our recent evolutionary past. The higher abundance of complex N-glycans in the human brain, for instance, appears to be the result of relatively steady incremental change over at least the last 80 million years since the divergence from rodents. In contrast, the shift toward greater use of α(2-6)–linked Neu5Ac seems to be nonlinear, with the greatest acceleration occurring in the more recent evolutionary past, primarily in the human lineage. While the selective pressures underpinning these differing rates of evolutionary change are still unknown, identifying and understanding them may provide clues regarding the neurobiological functions of individual N-glycosylation traits.

Regarding neurodevelopmental dynamics, we propose a model for the temporal transfiguration of the human brain N-glycome that incorporates elements of both global and region-specific maturation, leading to greater spatial diversification over the course of brain development (Fig. 10). We hypothesize that the changing neuroglycome reflects the evolving cellular landscape and functional requirements of a maturing organ (*27*). Some of these changes may arise because of changes in the cell composition of developing brain regions, such as the emergence of region-specific cell populations, and the resulting expression of cell-specific glycoproteins. For example, we hypothesize that the marked transformation of the cerebellar N-glycome is due to the emergence of granule cells, the majority of which appear postnatally (*50*).

N-glycosylation plays a pivotal role in numerous neurodevelopment processes, such as neural cell adhesion, neurite outgrowth, axon targeting, synaptogenesis, and synaptic plasticity (*10*). Its importance in brain development is illustrated by the prevalence of neurological symptoms that occur in many congenital disorders of glycosylation affecting N-glycan synthesis (*51*). Our work shows that some of the most notable developmental changes in brain N-glycosylation were related to the abundance, distribution, and linkage of Neu5Ac, a nutrient that is essential for brain development and cognition with a demonstrated role in learning and memory (*52*). The developmental trends in N-glycoprotein sialylation that we have identified here may be of clinical relevance because mutations in genes involved in either the synthesis (e.g., *GNE* and *NANS*) or recycling (e.g., *SLC17A5*) of Neu5Ac are associated with nervous system pathology, including developmental delay, seizures, and hypomyelination (*53*, *54*). Furthermore, dysfunction of the *ST3GAL3* gene, which encodes a sialyltransferase predominantly involved in synthesis of brain sialoglycoproteins (*55*), has been associated with intellectual disability in both animal models (*56*) and humans (*54*), highlighting this sialyltransferase and its glycoprotein substrates as key players in neurodevelopment. Our work supplements these findings by shining a spotlight on the types of N-glycan structures whose abundance is dynamically regulated during human brain development, thereby opening avenues for further research into the functional roles of specific N-glycans in neurodevelopment.

Many of the developmental trends and developmentally regulated N-glycans described here overlap with those seen in the rodent brain, suggesting that these may be conserved and, thus, important features of brain N-glycome maturation in mammals (*27*, *30*, *57*, *58*). However, our work has also uncovered some developmentally regulated N-glycans that have not previously been associated with brain development in rodents. This suggests that there are also species-specific differences in the regulation of individual N-glycan structures during neurodevelopment and further investigation of these carbohydrates, and their carrier glycoproteins may provide insights into aspects of brain development that are unique to different species. Ultimately, although glycomics studies still pose a methodological and analytical challenge, our findings demonstrate that an understanding of brain function, development, and evolution, including human-specific specializations, is incomplete without knowledge of the sugar modifications that are found on neural glycoproteins.

MATERIALS AND METHODS

Postmortem specimens

Information regarding the specimens used in this study is provided in table S1. For this study, we used fresh postmortem brain tissue (rats) or high-quality, histopathologically verified, neurotypical, fresh frozen brain tissue (primates). Tissue from all but one of the primate specimens has previously been used to generate other large-scale datasets in various modalities (exon arrays, mRNA-seq, small RNA-seq, single-cell RNA-seq, snRNA-seq, DNA methylation analysis, chromatin immunoprecipitation sequencing, and proteomics), and metadata regarding those specimens have been reported in earlier studies (*16*, *17*, *25*, *28*, *59*–*61*). Detailed descriptions of dissections and photo documentation are provided in these other studies. All experiments using nonhuman primates were carried out in accordance with a protocol approved by Yale University's Committee on Animal Research and National Institutes of Health (NIH) guidelines. The present study also complies with the definition of research exempt from the NIH Chimpanzee Research Use Panel (NOT-OD-14-024) regarding the use of chimpanzees or chimpanzee biomaterials. Following sample processing and data acquisition, samples not fulfilling quality control requirements were excluded. An overview of samples passing quality control is provided in table S2.

Human (Homo sapiens)

De-identified, clinically and neuropathologically unremarkable postmortem human brain tissue was procured from a bank of brain specimens; details regarding ethical approval and the collection process are reported in previous studies (*17*, *28*). Adult tissue was sourced from six donors (male, n = 3; female, n = 3) ranging from 23 to 82 years of age (median age, 36.5 years). Prenatal tissue was sourced from three mid-fetal donors (male, n = 1; female, n = 2) ranging from 21 to 23.5 PCW (median age, 21 PCW). Where possible, tissue was sampled from four different brain regions from each donor: the DFC, HIP, STR, and CBC. The median postmortem interval was 15 hours for adult specimens and 4 hours for fetal specimens.

Chimpanzee (Pan troglodytes)

Tissue samples were obtained from postmortem adult (age, 23 to 31 years) chimpanzee brains (male, n = 2; female, n = 2) according to criteria previously described (*17*). All chimpanzees suffered sudden death with no prolonged agonal state and for reasons other than their participation in this study and without any relation to the tissue used.

Rhesus macaque (Macaca mulatta)

Tissue samples from the appropriate brain regions were dissected from postmortem adult (age, 7 to 11 years) macaque brains (male, n = 3; female, n = 3) using criteria previously described (*17*). Rhesus macaques were euthanized for a previous study (*17*).

Rat (Rattus norvegicus)

Animals were obtained from the University of Zagreb School of Medicine and with the approval of the ethics committee of the University of Zagreb, Faculty of Science (approval number: 251-58-10617-15-20). Whole brains were isolated from 2-month-old Fisher 344 rats (male, n = 3; female, n = 3), and the appropriate brain regions were surgically microdissected. For the region corresponding to the primate DFC, the rat prefrontal cortex was dissected.

N-glycan release and labeling

An overview of workflow used in this study is provided in Fig. 1B. N-glycans were isolated from brain tissue, labeled with 2-AB, and prepared for chromatographic analysis as described previously (*14*), with minor modifications. Briefly, total protein content was isolated from brain tissue using chloroform/methanol extraction and denatured for 10 min at 95°C after which N-glycans were enzymatically released from glycoproteins using PNGase F (Promega, USA) over two overnight incubations at 37°C (5 U per incubation). The deglycosylation reactions were cleaned up using Amicon Ultra 2 mL Centrifugal Filter Devices (Merck Millipore, Germany) according to the manufacturer's instructions, and the purified N-glycans were labeled with 2-AB as previously reported (*62*). Free label and reducing agent were removed from the samples using a 0.2-μm GHP filter plate (Pall Corporation, USA). Glycans were eluted with ultrapure water (2× 90 μl) and stored at −20°C until use.

Ultraperformance liquid chromatography

Fluorescently labeled N-glycans were separated by HILIC on an Acquity UPLC instrument (Waters, USA) as described previously (*14*, *63*) with excitation and emission wavelengths of 250 and 428 nm, respectively. The instrument was under the control of Empower 3 software, build 3471 (Waters). Labeled N-glycans were separated on a Waters Ethylene Bridged Hybrid (BEH) Glycan chromatography column (150 mm by 2.1 mm, 1.7-μm BEH particles) with 100 mM ammonium formate (pH 4.4) as solvent A and acetonitrile as solvent B. The samples were run at a flow rate of 0.561 ml/min using a two-step linear gradient of 27 to 29.5% solvent A in the first 15 min and 29.5 to 38.7% for the next 80 min. Samples were maintained at 5°C before injection, and the separation temperature was 25°C. Data processing was performed using an automatic processing method with a traditional integration algorithm, after which each chromatogram was manually corrected to maintain the same intervals of integration for all the samples. The chromatograms were thus integrated into 58 peaks (chromatographic peaks 1 to 58). The glycan abundance in each peak was expressed as a percentage of total integrated area. Chromatographic peaks were assigned glucose unit (GU) values based on their retention time relative to 2-AB–labeled glucose oligomers of known length belonging to the external dextran ladder standard, as previously described (*64*).

Matrix-assisted laser desorption/ionization–time-of-flight/time-of-flight tandem mass spectrometry

The molecular masses of N-glycans were determined by MALDI-TOF/TOF MS/MS. Briefly, UPLC fractions corresponding to glycan peaks 1 to 58 were collected, dried, and resuspended in 2 to 5 μl of ultrapure water depending on the length of the fraction. Linkage-specific ethyl esterification of N-glycans was performed to stabilize sialylated N-glycans and distinguish α(2-3)– and α(2-6)–linked sialic acids as previously described (*65*). Following ethyl esterification, samples were cleaned up using cotton HILIC solid phase extraction as described previously (*66*), and the N-glycans were dried, resuspended in 2 μl of ultrapure water, spotted onto a MTP AnchorChip 384 BC MALDI target (Bruker Daltonics, Germany), mixed on plate with 1 μl of matrix solution [2,5-dihydroxybenzoic acid (5 mg/ml) and 1 mM sodium hydroxide in 50% acetonitrile], and left to air dry. Recrystallization was performed by adding 0.2 μl of ethanol to each spot. Analyses were performed in reflectron-positive (RP) mode on an ultrafleXtreme MALDI-TOF-MS equipped with a Smartbeam-II laser and flexControl 3.4 software Build 119 (Bruker Daltonics, Germany). The instrument was calibrated using a human plasma N-glycome standard. A 25-kV acceleration voltage was applied after a 140-ns extraction delay. A mass window of m/z 1000 to 5000 with suppression up to m/z 900 was used for brain N-glycan samples. For each spectrum, 10,000 laser shots were accumulated at a laser frequency of 2000 Hz using a complete sample random walk with 200 shots per raster spot. MS/MS was performed on the most abundant peaks via laser-induced disassociation. All raw MS and MS/MS data are available from the GlycoPOST repository (*67*) under the following accession numbers: rat (GPST000311), macaque (GPST000309), chimpanzee (GPST000310), adult human (GPST000308), and fetal human (GPST000312).

Annotation of chromatograms and assignment of proposed N-glycan structures to masses

The topological structure of N-glycans was deduced on the basis of the convergence of evidence from several different sources, as previously described (*27*). Figure S2 shows the approach used for assigning N-glycan structures to masses. Briefly, the GlycoMod software tool (*68*) was used to obtain a list of theoretically possible monosaccharide compositions for each detected monoisotopic mass. The following fixed modifications were used: reducing end 2-AB, sodiated (Na^+). Because it has been shown that fucose is the only 6-deoxyhexose present in rat brain glycoproteins (*69*), 6-deoxyhexose values are reported as fucose. The list of potential compositions for each segment was additionally filtered by cross-checking the GU value of the segment against reference values in the GlycoBase 3.2.4 database (*70*) to eliminate N-glycans that would not be expected to elute at the given retention time (e.g., glycan fragments generated by in-source fragmentation). Information about topological structure and the sequence of monosaccharides in the carbohydrate chain was deduced from diagnostic ions present in MS/MS fragmentation spectra, where available, which indicate specific N-glycan structural features and thus aided in distinguishing between isobaric isomers. Last, expert knowledge of the biosynthetic pathways involved in vertebrate N-glycan synthesis was coupled with evidence from the literature regarding the types of N-glycans present in brain tissue to provide an integrated approach to structural assignment. N-glycan structures were drawn using GlycoWorkbench (*71*) according to the standard symbol nomenclature for the representation of glycan structure proposed by the Consortium for Functional Glycomics (*72*).

Relative quantification of N-glycans and N-glycosylation traits

To make HILIC-UPLC measurements across samples comparable, normalization by total area was performed whereby the area of each of the 58 chromatographic peaks was divided by the total area of the corresponding chromatogram. Batch correction was performed on normalized log-transformed measurements using linear mixed models (R package lme4), in which the technical source of variation was modeled as a random effect. Before statistical analyses, N-glycan variables were all log-transformed because of right skewness of their distributions. In addition to directly measured glycan structures (i.e., peak abundance data for single chromatographic peaks), derived traits were calculated from the HILIC-UPLC data. These derived traits group together common glycosylation features across different individual chromatographic peaks, and consequently, they should be more closely associated with specific enzymatic pathways responsible for N-glycan synthesis. Because of qualitative differences in the N-glycan content of chromatographic peaks, derived N-glycosylation traits were calculated individually for each species, brain region, and developmental stage according to the formulas in table S7.

Analyses of differences in N-glycan–derived traits between sample groups were performed using the analysis of covariance (ANCOVA) model. When regional differences in N-glycosylation were analyzed within a single species, age and sex were included as additional covariates, while sex was included as a covariate when comparing N-glycomes across species. Correction for multiple testing was performed using the Bonferroni procedure.

Relative quantification of N-glycans within a chromatographic peak

For relative quantification of glycan peaks from MS spectra, absolute intensity values of the dominant isotopolog were manually extracted for each glycan composition in the spectrum, and glycan abundance was expressed as a percentage of the cumulative intensity. Glycan structures were excluded if their relative abundance was <10% in all samples (i.e., across all species and brain regions for evolutionary comparisons or across all developmental stages and brain regions for developmental comparisons).

Primate bulk transcriptomics data analysis

Complementary primate gene expression data from age-matched individuals was obtained from publicly available databases: Non-Human Primate Brain Transcriptomes (https://medicine.yale.edu/lab/sestan/resources/), National Chimpanzee Brain Resource (www.chimpanzeebrain.org), BrainSpan (www.brainspan.org) (*60*), and PsychENCODE (http://evolution.psychencode.org/#). For human samples, this corresponds to windows 4 and 9 for the mid-fetal and adult periods, respectively (*28*). Where possible, data from matching donors were used to complement the N-glycomic data and reduce noise introduced by interindividual variability (five of six adult human donors and eight of nine nonhuman primate donors were identical in both the N-glycomics and transcriptomics analyses; table S1). We obtained $\log_2$ reads per kilobase million (RPKM) expression data from human, chimpanzee, and macaque RNA-seq datasets for 47 glycogenes (table S9). In the adult brain, initial clustering revealed separation by species rather than brain regions. We z-scored expression values in each sample to express them as SDs from the mean expression of each sample. This transformation of the data rendered the expected clustering grouping first by region (particularly CBC and STR) and second by species. Fold changes and P values between fetal and adult were those determined by Li *et al.* (*60*) using DESeq2.

Digital droplet polymerase chain reaction

We used ddPCR to reliably quantitate gene expression and thus validate the bulk RNA-seq results. Briefly, 1 μg of total RNA was used for cDNA synthesis using SuperScript III First-strand synthesis Supermix (Invitrogen) and subsequently diluted with nuclease-free water. Custom gene-specific primers and probes for each gene of interest (table S9) were designed using National Center for Biotechnology Information (NCBI)/Primer-BLAST (www.ncbi.nlm.nih.gov/tools/primer-blast/) and PrimerQuest tool (IDT). ddPCR was carried out using the Bio-Rad QX100 system. After each PCR mixture consisting of ddPCR master mix and custom primers/probe set was partitioned into 15,000 to 20,000 droplets, parallel PCR amplification was carried out. Endpoint PCR signals were quantified, and Poisson statistics were applied to yield target copy number quantification of the sample. Two-color PCR reaction was used for the normalization of gene expression to the housekeeping gene *TBP*.

Proteomics analysis

Human, chimpanzee, and macaque DFC tissue was used for the proteomics experiment (n = 3 individuals per species). The DFC protein extraction, tryptic digestion, fractionation of peptides, and LC-MS/MS acquisition were done as described in our previous protocol (*16*). The raw files were searched against in-house–made species-specific databases of protein coding sequences (21,436, 21,693, and 21,213 protein entries for humans, chimpanzees, and macaques, respectively) in MaxQuant (2.03.01) (*73*) using the Andromeda search engine. Carbamidomethylation was set as a fixed modification, and N-terminal acetylation and oxidation of methionine were used as variable modifications. Maximum two trypsin/P missed cleavages, a tolerance of 10 parts per million for precursor mass, a tolerance of 0.5 Da for fragment ions, and match between runs were set for protein searches. A maximum of 1% false discovery rate was set for both protein and peptide identification. The contaminants and reverse proteins were removed using Perseus version 2.0.7.0 (*74*).

A list of all 47 glycoenzymes and 470 control proteins investigated can be found in table S10. Control proteins are a random sample of all annotated proteins in the respective proteomes and are well detected proteomically (average number of peptides ± SEM; human, 14.7 ± 1; chimpanzee, 11.9 ± 0.8; macaque, 12.2 ± 0.9). The mean and median protein lengths of the control proteins are similar to those of all proteins in the proteome and to glycoenzymes (table S10). The control proteins are also of a similar age compared to glycoenzymes, and their amino acid sequences are equally well conserved compared to glycoenzymes as determined by the proportion of the protein sequence aligned between species (table S10). The plots were made in GraphPad Prism version 9.4.0. Heatmaps were generated in Heatmapper software (*75*). The Mann-Whitney and Fisher′s exact tests were used to determine the statistical significance of differences between different categories.

Estimation of gene age

For the three primate species, we retrieved all protein sequences from the NCBI database (www.ncbi.nlm.nih.gov/protein/) and estimated the evolutionary age of protein-coding genes by phylostratigraphy (*76*, *77*), which classifies genes on the basis of their taxonomic restriction (*78*). For every gene encoding a protein of at least 40 amino acids, the protein sequence is used to query the largest possible reference database, such as the NCBI NR database and determine the most distant species in which a sufficiently similar protein sequence exists (*78*), as evaluated by BLASTP (*79*) and HMMER (*80*). The minimal age of the gene is evaluated as the time of the evolutionary node, retrieved from NCBI Taxonomy, when the most recent common ancestor of the query species and the most distant species lived. Node age is evaluated with TimeTree (*81*). Thus, a human gene also present in bacteria is in phylostratum 1 (ancestor at the first node; Cellular Organisms) and thus ancient. A human gene also present in zebrafish, but not more distant species, is chordate specific. A human gene shared with platypus is mammal specific. A human gene shared with lemurs is primate specific; a human gene present only in humans is in phylostratum 31, and is human-specific. For each of these three primate species, one protein isoform per gene (encoding the longest and oldest protein sequence) was kept to build species-specific databases of protein coding sequences for peptide searches.

ST3GAL2 immunohistochemistry

For validation experiments, prefrontal cortex, dorsal STR, and CBC were dissected from adult human, rhesus macaque, and chimpanzee specimens (n = 1 biological replicate from each species), sectioned at 50-μm thickness on a Leica VT1000s vibratome, and mounted on TOMO adhesion slides (Matsunami Glass USA, #TOM-11/90).

Antigen retrieval was performed with the Retriever 2100 (Electron Microscopy Services) using Buffer A pH 6.0 (EMS #62706-10) for the prefrontal cortex and CBC, and using Buffer AG pH 6.0 (EMS #62707-10) for STR according to the manufacturer's instructions. Tissue sections were washed in phosphate-buffered saline (PBS) (3 × 2 min) and incubated in 3% hydrogen peroxide/PBS to quench endogenous peroxidase activity. Sections were washed in PBS (3 × 2 min) and incubated in blocking solution containing 5% (v/v) normal donkey serum (Jackson ImmunoResearch Laboratories), 1% (w/v) bovine serum albumin, and 0.3% (v/v) Triton X-100 in PBS for 30 min at room temperature. ST3GAL2 primary antibody (Abcam, #ab254726) was diluted 1:200 in blocking solution and incubated with tissue sections at 4°C for two nights (prefrontal cortex and CBC) or overnight (STR). Sections were washed with 1× PBS + 0.3% Triton X-100 (PBST) for 3 × 5 min before being incubated for 1 hour at room temperature with a goat anti-rabbit peroxidase-conjugated secondary antibody (Jackson ImmunoResearch Labs) diluted at 1:250 in blocking solution. Sections were washed in PBST (3 × 5 min) and tyramide signal amplification was performed with TSA Plus Fluorescein (Akoya Biosciences, #NEL741001KT) or TSA Plus Cy3 (Akoya Biosciences, #NEL744001KT) diluted 1:200 in 1× Plus Amplification Diluent (Akoya Biosciences, #FP1135) for 10 min at room temperature. Sections were washed in PBST, treated with Autofluorescence Eliminator Reagent (Millipore #2160), and cover-slipped with Vectashield Plus (Vector Laboratories, #H-1900).

Imaging and quantification of ST3GAL2 immunolabeled cells

To quantify species differences in ST3GAL2 expression, *z*-stack confocal images were acquired using a Nikon A1 confocal microscope. For the prefrontal cortex, 10 high-resolution (1024 × 1024 pixels; zoom, 1.25; pixel size, 0.50 μm) z-stack images were acquired from each section with 2-μm step size and high and low *z*-position limits set above and below the section focal plane, respectively, using a 20× objective (Plan Apo, numerical aperture 0.75, working distance 1 mm). To quantify differences in STR ST3GAL2 expression, five high-resolution (1024 × 1024 pixels; zoom, 1.00; pixel size, 0.21 μm) *z*-stack images were acquired from each section with 2-μm step size and high and low *z*-position limits set above and below the section focal plane, respectively, using a 60× objective (Plan Apo, numerical aperture 1.4; working distance 130 μm). For CBC quantification, five high-resolution (1024 × 1024 pixels; zoom, 1.00; pixel size, 0.21 μm) *z*-stack images were acquired from the molecular layer, Purkinje cell layer, and granule cell layer from each section with 2-μm step size and high and low *z*-position limits set above and below the section focal plane, respectively, using a 60× objective (Plan Apo, numerical aperture 1.4; working distance, 130 μm). For each brain region, identical laser power and detector gain settings were used. The images were blinded and randomized before quantification and the number of $ST3GAL2^{+}/DAPI^{+}$ cells counted manually for each brain region.

Primate snRNA-seq data analysis

Complementary primate DFC snRNA-seq expression data were obtained from a previously published study (*25*). Here, the differential expression analysis was performed between each pair of species in a given homologous cell cluster using the FindMarkers function in Seurat (*82*), with the significance evaluated by Wilcoxon rank sum test. Pie charts were used to summarize the expression patterns across species. We further clustered the glycogenes on the basis of their expression patterns across cell clusters and species. Specifically, we calculated the average expression of each glycogene in each cell cluster and species using the AverageExpression function in Seurat followed by log transformation. We then calculated the Spearman correlation coefficients between each pair of genes and defined the gene-gene distance by subtracting the coefficients from 1. The gene-gene distance matrix was passed to hclust function in R with the "ward.D2" algorithm to construct the dendrogram hierarchically organizing the glycogenes. For a global overview of the species divergence in glycogene expression, we measured the Pearson correlation coefficients of the average expression of glycogenes in a given homologous cell cluster between each pair of species, followed by subtracting from 1 to represent expression dissimilarity. The dissimilarities were visualized in Fig. 8C.

Linear regression and quantile-quantile plot

In each brain region, a linear model was performed for the glycans abundance against the evolutionary age using the lm function in R. To evaluate the normality of the data across species, we obtained the standardized quantiles of the observed data via the rstandard function in R, calculated the theoretical Gaussian quantiles, and plotted the results in dot plots (quantile-quantile plot) with dots colored by species.

Correlation of the N-glycome and glycotranscriptome within and among primate species

To avoid species/batch confounding effects in gene expression and peak abundance, we calculated pairwise correlation matrices in glycogenes and peaks. Coexpression/coabundance matrices were correlated between species using the Mantel test implemented in the ade4 R package. To test the significance of these correlations, we resampled groups of 47 genes 1000 times and obtained a distribution of Mantel's correlations between species. In matching samples, we also calculated the correlation between peaks and glycogenes independently in each species. To test how well the relationships between peaks and glycogenes were conserved, we then calculated the correlation of these Pearson's coefficients between species.

We further analyzed the relationship between glycogenes and peaks in human development using sparse partial least squares implemented in the mixOmics R package (*83*). We used two components to calculate the correlation structure between the abundance of glycan peaks and the expression of glycogenes measured in humans. We visualized relationships between glycogenes and peaks in a network using the igraph package in R, removing unconnected nodes, and edges with correlations smaller than 0.6. Data were analyzed and visualized using R programming language (version 3.0.1).

Calculation of the glycogene specificity score

For each human brain region and time period (fetal and adult), we encoded the putative involvement between each glycogene and the dominant N-glycan structure in each individual N-glycan peak with a binary entry (1/0 for evidence/no evidence) based on common knowledge of N-glycan biosynthetic pathways (*84*) in conjunction with available information regarding enzyme activity (*55*). For each glycogene, we calculated a specificity score describing how specific the relationship is between the glycogene and a certain N-glycan peak, considering the involvement of the glycogene with the rest of the peaks. The score was calculated as

$$S_z = \frac{\sum_{i}^{n} z - x_i}{n - 1}$$

where S_z is the specificity score of a particular glycogene-peak relationship, Z is the evidence for functional relationship glycogene peak, and x_i all possible (n) relationships.

Data analysis, visualization, and presentation

GraphPad Prism 8.4.3 was used for drawing graphs and the following basic statistical tests and analyses: *t* tests, analysis of variance (ANOVA), mixed model analysis, and PCA with the exception of the PCA of the global N-glycome across human neurodevelopment which was performed using the analysis and visualization software BioVinci (version 1.1.5, r20181005). BioVinci was also used for *t*-SNE analysis and hierarchical clustering. The complete-linkage method and Euclidean distancing parameters were used for hierarchical clustering. GlyConnect Compozitor (1.0.0) was used to construct the core brain N-glycan network (*85*) with the assumption that the core N-glycan structures are biosynthetically interrelated and are the products of a small number of N-glycan processing pathways that are dominant in the brain. Accordingly, the illustrated N-glycans depict the proposed structural configurations while also taking into account GU value, knowledge of N-glycan biosynthetic pathways, information from the literature, and MALDI-TOF/TOF MS/MS fragmentation spectra (where available). Icons from BioRender were used for drawing figures.

Supplementary Materials

This PDF file includes:
Supplementary Text
Figs. S1 to S47
Legends for tables S1 to S11
References

Other Supplementary Material for this manuscript includes the following:
Tables S1 to S11

REFERENCES AND NOTES

1. A. M. M. Sousa, K. A. Meyer, G. Santpere, F. O. Gulden, N. Sestan, Evolution of the human nervous system function, structure, and development. *Cell* **170**, 226–247 (2017).
2. R. S. Hill, C. A. Walsh, Molecular insights into human brain evolution. *Nature* **437**, 64–67 (2005).
3. P. Khaitovich, W. Enard, M. Lachmann, S. Pääbo, Evolution of primate gene expression. *Nat. Rev. Genet.* **7**, 693–702 (2006).
4. G. Konopka, D. H. Geschwind, Human brain evolution: Harnessing the genomics (r)evolution to link genes, cognition, and behavior. *Neuron* **68**, 231–244 (2010).
5. T. M. Preuss, Human brain evolution: From gene discovery to phenotype discovery. *Proc. Natl. Acad. Sci. U.S.A.* **109**, 10709–10716 (2012).
6. C. C. Sherwood, A. L. Bauernfeind, S. Bianchi, M. A. Raghanti, P. R. Hof, Human brain evolution writ large and small. *Prog. Brain Res.* **195**, 237–254 (2012).
7. A. A. Pollen, A. Bhaduri, M. G. Andrews, T. J. Nowakowski, O. S. Meyerson, M. A. Mostajo-Radji, E. Di Lullo, B. Alvarado, M. Bedolli, M. L. Dougherty, I. T. Fiddes, Z. N. Kronenberg, J. Shuga, A. A. Leyrat, J. A. West, M. Bershteyn, C. B. Lowe, B. J. Pavlovic, S. R. Salama, D. Haussler, E. E. Eichler, A. R. Kriegstein, Establishing cerebral organoids as models of human-specific brain evolution. *Cell* **176**, 743–756 (2019).
8. T. Namba, J. Nardelli, P. Gressens, W. B. Huttner, Metabolic regulation of neocortical expansion in development and evolution. *Neuron* **109**, 408–419 (2021).
9. P. Gagneux, M. Aebi, A. Varki, in *Essentials of Glycobiology*, A. Varki, R.D. Cummings, J.D. Esko, Eds. (Cold Spring Harbor Laboratory Press, 2015), pp. 253–264.
10. R.K. Yu, C.-L. Schengrund, Eds., *Glycobiology of the Nervous System* (Springer, ed. 1, 2014), vol. 9 of *Advances in Neurobiology*.
11. L. R. Conroy, T. R. Hawkinson, L. E. A. Young, M. S. Gentry, R. C. Sun, Emerging roles of N-linked glycosylation in brain physiology and disorders. *Trends Endocrinol. Metab.* **32**, 980–993 (2021).
12. T. S. Klarić, G. Lauc, The dynamic brain N-glycome. *Glycoconj. J.* **39**, 443–471 (2022).
13. J. Lee, S. Ha, M. Kim, S.-W. Kim, J. Yun, S. Ozcan, H. Hwang, I. J. Ji, D. Yin, M. J. Webster, C. S. Weickert, J.-H. Kim, J. S. Yoo, R. Grimm, S. Bahn, H.-S. Shin, H. J. An, Spatial and temporal diversity of glycome expression in mammalian brain. *Proc. Natl. Acad. Sci. U.S.A.* **117**, 28743–28753 (2020).
14. T. Klarić, I. Gudelj, HILIC-UPLC analysis of brain tissue N-glycans. *Methods Mol. Biol.* **1503**, 207–216 (2017).
15. S. E. Williams, M. Noel, S. Lehoux, M. Cetinbas, R. J. Xavier, R. I. Sadreyev, E. M. Scolnick, J. W. Smoller, R. D. Cummings, R. G. Mealer, Mammalian brain glycoproteins exhibit diminished glycan complexity compared to other tissues. *Nat. Commun.* **13**, 275 (2022).
16. B. C. Carlyle, R. R. Kitchen, J. E. Kanyo, E. Z. Voss, M. Pletikos, A. M. M. Sousa, T. K. T. Lam, M. B. Gerstein, N. Sestan, A. C. Nairn, A multiregional proteomic survey of the postnatal human brain. *Nat. Neurosci.* **20**, 1787–1795 (2017).
17. A. M. M. Sousa, Y. Zhu, M. A. Raghanti, R. R. Kitchen, M. Onorati, A. T. N. Tebbenkamp, B. Stutz, K. A. Meyer, M. Li, Y. I. Kawasawa, F. Liu, R. G. Perez, M. Mele, T. Carvalho, M. Skarica, F. O. Gulden, M. Pletikos, A. Shibata, A. R. Stephenson, M. K. Edler, J. J. Ely, J. D. Elsworth, T. L. Horvath, P. R. Hof, T. M. Hyde, J. E. Kleinman, D. R. Weinberger, M. Reimers, R. P. Lifton, S. M. Mane, J. P. Noonan, M. W. State, E. S. Lein, J. A. Knowles, T. Marques-Bonet, C. C. Sherwood, M. B. Gerstein, N. Sestan, Molecular and cellular reorganization of neural circuits in the human lineage. *Science* **358**, 1027–1032 (2017).
18. M. Binder, N. Hirokawa, U. Windhorst, Eds., *Encyclopedia of Neuroscience* (Springer, 2009).
19. K. Bozek, Y. Wei, Z. Yan, X. Liu, J. Xiong, M. Sugimoto, M. Tomita, S. Pääbo, C. C. Sherwood, P. R. Hof, J. J. Ely, Y. Li, D. Steinhauser, L. Willmitzer, P. Giavalisco, P. Khaitovich, Organization and evolution of brain lipidome revealed by large-scale analysis of human, chimpanzee, macaque, and mouse tissues. *Neuron* **85**, 695–702 (2015).
20. L. Montanucci, H. Laayouni, G. M. Dall'Olio, J. Bertranpetit, Molecular evolution and network-level analysis of the N-glycosylation metabolic pathway across primates. *Mol. Biol. Evol.* **28**, 813–823 (2011).
21. S. Neelamegham, L. K. Mahal, Multi-level regulation of cellular glycosylation: From genes to transcript to enzyme to structure. *Curr. Opin. Struct. Biol.* **40**, 145–152 (2016).
22. A. V. Nairn, W. S. York, K. Harris, E. M. Hall, J. M. Pierce, K. W. Moremen, Regulation of glycan structures in animal tissues: Transcript profiling of glycan-related genes. *J. Biol. Chem.* **283**, 17298–17313 (2008).
23. J. E. Froberg, O. Durak, J. D. Macklis, Development of nanoRibo-seq enables study of regulated translation by cortical neuron subtypes, showing uORF translation in synaptic-axonal genes. *Cell Rep.* **42**, 112995 (2023).
24. P. Gagneux, A. Varki, Evolutionary considerations in relating oligosaccharide diversity to biological function. *Glycobiology* **9**, 747–755 (1999).
25. S. Ma, M. Skarica, Q. Li, C. Xu, R. D. Risgaard, A. T. N. Tebbenkamp, X. Mato-Blanco, R. Kovner, Ž. Krsnik, X. de Martin, V. Luria, X. Martí-Pérez, D. Liang, A. Karger, D. K. Schmidt, Z. Gomez-Sanchez, C. Qi, K. T. Gobeske, S. Pochareddy, A. Debnath, C. J. Hottman, J. Spurrier, L. Teo, A. G. Boghdadi, J. Homman-Ludiye, J. J. Ely, E. W. Daadi, D. Mi, M. Daadi, O. Marín, P. R. Hof, M.-R. Rasin, J. Bourne, C. C. Sherwood, G. Santpere, M. J. Girgenti, S. M. Strittmatter, A. M. M. Sousa, N. Sestan, Molecular and cellular evolution of the primate dorsolateral prefrontal cortex. *Science* **377**, eabo7257 (2022).
26. A. D. Workman, C. J. Charvet, B. Clancy, R. B. Darlington, B. L. Finlay, Modeling transformations of neurodevelopmental sequences across mammalian species. *J. Neurosci.* **33**, 7368–7383 (2013).
27. T. S. Klarić, M. Salopek, V. Micek, O. Gornik Kljaić, G. Lauc, Post-natal developmental changes in the composition of the rat neocortical N-glycome. *Glycobiology* **31**, 636–648 (2021).
28. H. J. Kang, Y. I. Kawasawa, F. Cheng, Y. Zhu, X. Xu, M. Li, A. M. M. Sousa, M. Pletikos, K. A. Meyer, G. Sedmak, T. Guennel, Y. Shin, M. B. Johnson, Ž. Krsnik, S. Mayer, S. Fertuzinhos, S. Umlauf, S. N. Lisgo, A. Vortmeyer, D. R. Weinberger, S. Mane, T. M. Hyde, A. Huttner, M. Reimers, J. E. Kleinman, N. Sestan, Spatio-temporal transcriptome of the human brain. *Nature* **478**, 483–489 (2011).
29. S. C. Fu, J. W. Gurd, Developmental changes in the oligosaccharide composition of synaptic junctional glycoproteins. *J. Neurochem.* **41**, 1726–1734 (1983).

30. A. Ishii, T. Ikeda, S. Hitoshi, I. Fujimoto, T. Torii, K. Sakuma, S.-i. Nakakita, S. Hase, K. Ikenaka, Developmental changes in the expression of glycogenes and the content of N-glycans in the mouse cerebral cortex. *Glycobiology* **17**, 261–276 (2007).
31. T. Torii, T. Yoshimura, M. Narumi, S. Hitoshi, Y. Takaki, S. Tsuji, K. Ikenaka, Determination of major sialylated N-glycans and identification of branched sialylated N-glycans that dynamically change their content during development in the mouse cerebral cortex. *Glycoconj. J.* **31**, 671–683 (2014).
32. F. Schwarz, M. Aebi, Mechanisms and principles of N-linked protein glycosylation. *Curr. Opin. Struct. Biol.* **21**, 576–582 (2011).
33. C. Hanus, H. Geptin, G. Tushev, S. Garg, B. Alvarez-Castelao, S. Sambandan, L. Kochen, A.-S. Hafner, J. D. Langer, E. M. Schuman, Unconventional secretory processing diversifies neuronal ion channel properties. *eLife* **5**, e20609 (2016).
34. C.-L. Schengrund, Roles of carbohydrates in the interaction of pathogens with neural cells. *Adv. Neurobiol.* **9**, 395–413 (2014).
35. S. M. Reader, Y. Hager, K. N. Laland, The evolution of primate general and cultural intelligence. *Philos. Trans. R. Soc. B Biol. Sci.* **366**, 1017–1027 (2011).
36. C. Heyes, New thinking: The evolution of human cognition. *Philos. Trans. R. Soc. Lond. B Biol. Sci.* **367**, 2091–2096 (2012).
37. E. L. MacLean, Unraveling the evolution of uniquely human cognition. *Proc. Natl. Acad. Sci. U.S.A.* **113**, 6348–6354 (2016).
38. S. T. Gizaw, T. Koda, M. Amano, K. Kamimura, T. Ohashi, H. Hinou, S. I. Nishimura, A comprehensive glycome profiling of Huntington's disease transgenic mice. *Biochim. Biophys. Acta.* **1850**, 1704–1718 (2015).
39. J. Samal, R. Saldova, P. M. Rudd, A. Pandit, R. O'Flaherty, Region-specific characterization of N-glycans in the striatum and substantia nigra of an adult rodent brain. *Anal. Chem.* **92**, 12842–12851 (2020).
40. C. L. Fazekas, E. Sipos, T. Klaric, B. Török, M. Bellardie, G. N. Erjave, M. N. Perkovic, G. Lauc, N. Pivac, D. Zelena, Searching for glycomic biomarkers for predicting resilience and vulnerability in a rat model of posttraumatic stress disorder. *Stress* **23**, 715–731 (2020).
41. M. Barboza, K. Solakyildirim, T. A. Knotts, J. Luke, M. G. Gareau, H. E. Raybould, C. B. Lebrilla, Region-specific cell membrane N-glycome of functional mouse brain areas revealed by nanoLC-MS analysis. *Mol. Cell. Proteomics* **20**, 100130 (2021).
42. N. Yamakawa, J. Vanbeselaere, L.-Y. Chang, S.-Y. Yu, L. Ducrocq, A. Harduin-Lepers, J. Kurata, K. F. Aoki-Kinoshita, C. Sato, K.-H. Khoo, K. Kitajima, Y. Guerardel, Systems glycomics of adult zebrafish identifies organ-specific sialylation and glycosylation patterns. *Nat. Commun.* **9**, 4647 (2018).
43. T. R. Hawkinson, H. A. Clarke, L. E. A. Young, L. R. Conroy, K. H. Markussen, K. M. Kerch, L. A. Johnson, P. T. Nelson, C. Wang, D. B. Allison, M. S. Gentry, R. C. Sun, In situ spatial glycomic imaging of mouse and human Alzheimer's disease brains. *Alzheimers Dement.* **18**, 1721–1735 (2022).
44. S. Gaunitz, L. O. Tjernberg, S. Schedin-Weiss, The N-glycan profile in cortex and hippocampus is altered in Alzheimer disease. *J. Neurochem.* **159**, 292–304 (2021).
45. N. M. Varki, E. Strobert, E. J. Dick, K. Benirschke, A. Varki, Biomedical differences between human and nonhuman hominids: Potential roles for uniquely human aspects of sialic acid biology. *Annu. Rev. Pathol.* **6**, 365–393 (2011).
46. P. Gagneux, M. Cheriyan, N. Hurtado-Ziola, E. C. M. Brinkman Van Der Linden, D. Anderson, H. McClure, A. Varki, N. M. Varki, Human-specific regulation of α2-6-linked sialic acids. *J. Biol. Chem.* **278**, 48245–48250 (2003).
47. D. Bojar, L. Meche, G. Meng, W. Eng, D. F. Smith, R. D. Cummings, L. K. Mahal, A useful guide to lectin binding: Machine-learning directed annotation of 57 unique lectin specificities. *ACS Chem. Biol.* **17**, 2993–3012 (2022).
48. M.-A. Krzewinski-Recchi, S. Julien, S. Juliant, M. Teintenier-Lelièvre, B. Samyn-Petit, M.-D. Montiel, A.-M. Mir, M. Cerutti, A. Harduin-Lepers, P. Delannoy, Identification and functional expression of a second human β-galactoside α2,6-sialyltransferase, ST6Gal II. *Eur. J. Biochem.* **270**, 950–961 (2003).
49. H. Jang, D. Boltz, K. Sturm-Ramirez, K. R. Shepherd, Y. Jiao, R. Webster, R. J. Smeyne, Highly pathogenic H5N1 influenza virus can enter the central nervous system and induce neuroinflammation and neurodegeneration. *Proc. Natl. Acad. Sci. U.S.A.* **106**, 14063–14068 (2009).
50. M. C. Kiessling, A. Büttner, C. Butti, J. Müller-Starck, S. Milz, P. R. Hof, H. G. Frank, C. Schmitz, Cerebellar granule cells are generated postnatally in humans. *Brain Struct. Funct.* **219**, 1271–1286 (2014).
51. H. H. Freeze, E. A. Eklund, B. G. Ng, M. C. Patterson, Neurological aspects of human glycosylation disorders. *Annu. Rev. Neurosci.* **38**, 105–125 (2015).
52. B. Wang, Molecular mechanism underlying sialic acid as an essential nutrient for brain development and cognition. *Adv. Nutr.* **3**, 465S–472S (2012).
53. C. D. M. van Karnebeek, L. Bonafé, X.-Y. Wen, M. Tarailo-Graovac, S. Balzano, B. Royer-Bertrand, A. Ashikov, L. Garavelli, I. Mammi, L. Turolla, C. Breen, D. Donnai, V. Cormier-Daire, D. Heron, G. Nishimura, S. Uchikawa, B. Campos-Xavier, A. Rossi, T. Hennet, K. Brand-Arzamendi, J. Rozmus, K. Harshman, B. J. Stevenson, E. Girardi, G. Superti-Furga, T. Dewan, A. Collingridge, J. Halparin, C. J. Ross, M. I. Van Allen, A. Rossi, U. F. Engelke, L. A. J. Kluijtmans, E. van der Heeft, H. Renkema, A. de Brouwer, K. Huijben, F. Zijlstra, T. Heise, T. Boltje, W. W. Wasserman, C. Rivolta, S. Unger, D. J. Lefeber, R. A. Wevers, A. Superti-Furga, NANS-mediated synthesis of sialic acid is required for brain and skeletal development. *Nat. Genet.* **48**, 777–784 (2016).
54. R. L. Schnaar, R. Gerardy-Schahn, H. Hildebrandt, Sialic acids in the brain: Gangliosides and polysialic acid in nervous system development, stability, disease, and regeneration. *Physiol. Rev.* **94**, 461–518 (2014).
55. N. Taniguchi, K. Honke, M. Fukuda, H. Narimatsu, Y. Yamaguchi, T. Angata, *Handbook of Glycosyltransferases and Related Genes* (Springer Reference, ed. 2, 2014), vol. 1–2.
56. S.-W. Yoo, M. G. Motari, K. Susuki, J. Prendergast, A. Mountney, A. Hurtado, R. L. Schnaar, Sialylation regulates brain structure and function. *FASEB J.* **29**, 3040–3053 (2015).
57. T. Krusius, J. Finne, J. Kärkkäinen, J. Järnefelt, Neutral and acidic glycopeptides in adult and developing rat brain. *Biochim. Biophys. Acta.* **365**, 80–92 (1974).
58. R. K. Margolis, C. Preti, D. Lai, R. U. Margolis, Developmental changes in brain glycoproteins. *Brain Res.* **112**, 363–369 (1976).
59. Y. Zhu, A. M. M. Sousa, T. Gao, M. Skarica, M. Li, G. Santpere, P. Esteller-Cucala, D. Juan, L. Ferrández-Peral, F. O. Gulden, M. Yang, D. J. Miller, T. Marques-Bonet, Y. I. Kawasawa, H. Zhao, N. Sestan, Spatiotemporal transcriptomic divergence across human and macaque brain development. *Science* **362**, eaat8077 (2018).
60. M. Li, G. Santpere, Y. I. Kawasawa, O. V. Evgrafov, F. O. Gulden, S. Pochareddy, S. M. Sunkin, Z. Li, Y. Shin, Y. Zhu, A. M. M. Sousa, D. M. Werling, R. R. Kitchen, H. J. Kang, M. Pletikos, J. Choi, S. Muchnik, X. Xu, D. Wang, B. Lorente-Galdos, S. Liu, P. Giusti-Rodríguez, H. Won, C. A. de Leeuw, A. F. Pardiñas, B. S. Consortium, M. Hu, F. Jin, Y. Li, M. J. Owen, M. C. O'Donovan, J. T. R. Walters, D. Posthuma, M. A. Reimers, P. Levitt, D. R. Weinberger, T. M. Hyde, J. E. Kleinman, D. H. Geschwind, M. J. Hawrylycz, M. W. State, S. J. Sanders, P. F. Sullivan, M. B. Gerstein, E. S. Lein, J. A. Knowles, N. Sestan, Psych ENCODE ConsortiumPsych ENCODE Developmental Subgroup, Integrative functional genomic analysis of human brain development and neuropsychiatric risks. *Science*, **362**, eaat7615 (2018).
61. M. Pletikos, A. M. M. Sousa, G. Sedmak, K. A. Meyer, Y. Zhu, F. Cheng, M. Li, Y. I. Kawasawa, N. Sestan, Temporal specification and bilaterality of human neocortical topographic gene expression. *Neuron* **81**, 321–332 (2014).
62. I. T. Akmačić, I. Ugrina, J. Štambuk, I. Gudelj, F. Vučković, G. Lauc, M. P. Baković, High-throughput glycomics: Optimization of sample preparation. *Biochemistry* **80**, 934–942 (2015).
63. M. Vacchini, L. Cipolla, O. Gornik, G. Lauc, T. Klarić, A precise and versatile platform for rapid glycosylation analysis of brain tissue. *Anal. Methods* **12**, 1786–1797 (2020).
64. G. R. Guile, P. M. Rudd, D. R. Wing, S. B. Prime, R. A. Dwek, A rapid high-resolution high-performance liquid chromatographic method for separating glycan mixtures and analyzing oligosaccharide profiles. *Anal. Biochem.* **240**, 210–226 (1996).
65. K. R. Reiding, E. Lonardi, A. L. Hipgrave Ederveen, M. Wuhrer, Ethyl esterification for MALDI-MS analysis of protein glycosylation. *Methods Mol. Biol.* **1394**, 151–162 (2016).
66. K. R. Reiding, D. Blank, D. M. Kuijper, A. M. Deelder, M. Wuhrer, High-throughput profiling of protein N-glycosylation by MALDI-TOF-MS employing linkage-specific sialic acid esterification. *Anal. Chem.* **86**, 5784–5793 (2014).
67. Y. Watanabe, K. F. Aoki-Kinoshita, Y. Ishihama, S. Okuda, GlycoPOST realizes FAIR principles for glycomics mass spectrometry data. *Nucleic Acids Res.* **49**, D1523–D1528 (2021).
68. C. A. Cooper, E. Gasteiger, N. H. Packer, GlycoMod—A software tool for determining glycosylation compositions from mass spectrometric data. *Proteomics* **1**, 340–349 (2001).
69. E. G. Brunngraber, B. D. Brown, Fractionation of brain macromolecules—II. Isolation of protein-linked sialomucopoly-saccharides from subcellular, particulate fractions from rat brain. *J. Neurochem.* **11**, 449–459 (1964).
70. M. P. Campbell, L. Royle, C. M. Radcliffe, R. A. Dwek, P. M. Rudd, GlycoBase and autoGU: Tools for HPLC-based glycan analysis. *Bioinformatics* **24**, 1214–1216 (2008).
71. A. Ceroni, K. Maass, H. Geyer, R. Geyer, A. Dell, S. M. Haslam, GlycoWorkbench: A tool for the computer-assisted annotation of mass spectra of glycans. *J. Proteome Res.* **7**, 1650–1659 (2008).
72. A. Varki, R. D. Cummings, J. D. Esko, H. H. Freeze, P. Stanley, J. D. Marth, C. R. Bertozzi, G. W. Hart, M. E. Etzler, Symbol nomenclature for glycan representation. *Proteomics* **9**, 5398–5399 (2009).
73. J. Cox, N. Neuhauser, A. Michalski, R. A. Scheltema, J. V. Olsen, M. Mann, Andromeda: A peptide search engine integrated into the MaxQuant environment. *J. Proteome Res.* **10**, 1794–1805 (2011).
74. S. Tyanova, T. Temu, P. Sinitcyn, A. Carlson, M. Y. Hein, T. Geiger, M. Mann, J. Cox, The Perseus computational platform for comprehensive analysis of (prote)omics data. *Nat. Methods* **13**, 731–740 (2016).
75. S. Babicki, D. Arndt, A. Marcu, Y. Liang, J. R. Grant, A. Maciejewski, D. S. Wishart, Heatmapper: Web-enabled heat mapping for all. *Nucleic Acids Res.* **44**, W147–W153 (2016).

76. T. Domazet-Lošo, J. Brajković, D. Tautz, A phylostratigraphy approach to uncover the genomic history of major adaptations in metazoan lineages. *Trends Genet.* **23**, 533–539 (2007).
77. T. Domazet-Lošo, A. R. Carvunis, M. M. Albà, M. S. Šestak, R. Bakarić, R. Neme, D. Tautz, Y. Kim, No evidence for phylostratigraphic bias impacting inferences on patterns of gene emergence and evolution. *Mol. Biol. Evol.* **34**, 843–856 (2017).
78. J. A. Weber, S. G. Park, V. Luria, S. Jeon, H. M. Kim, Y. Jeon, Y. Bhak, J. H. Jun, S. W. Kim, W. H. Hong, S. Lee, Y. S. Cho, A. Karger, J. W. Cain, A. Manica, S. Kim, J. H. Kim, J. S. Edwards, J. Bhak, G. M. Church, The whale shark genome reveals how genomic and physiological properties scale with body size. *Proc. Natl. Acad. Sci. U.S.A.* **117**, 20662–20671 (2020).
79. S. F. Altschul, W. Gish, W. Miller, E. W. Myers, D. J. Lipman, Basic local alignment search tool. *J. Mol. Biol.* **215**, 403–410 (1990).
80. S. El-Gebali, J. Mistry, A. Bateman, S. R. Eddy, A. Luciani, S. C. Potter, M. Qureshi, L. J. Richardson, G. A. Salazar, A. Smart, E. L. L. Sonnhammer, L. Hirsh, L. Paladin, D. Piovesan, S. C. E. Tosatto, R. D. Finn, The Pfam protein families database in 2019. *Nucleic Acids Res.* **47**, D427–D432 (2019).
81. S. Kumar, G. Stecher, M. Suleski, S. Blair Hedges, TimeTree: A resource for timelines, timetrees, and divergence times. *Mol. Biol. Evol.* **34**, 1812–1819 (2017).
82. T. Stuart, A. Butler, P. Hoffman, C. Hafemeister, E. Papalexi, W. M. Mauck, Y. Hao, M. Stoeckius, P. Smibert, R. Satija, Comprehensive integration of single-cell data. *Cell* **177**, 1888–1902.e21 (2019).
83. K. A. Lê Cao, D. Rossouw, C. Robert-Granié, P. Besse, A sparse PLS for variable selection when integrating omics data. *Stat. Appl. Genet. Mol. Biol.* **7**, Article 35 (2008).
84. A. Varki, R.D. Cummings, J. D. Esko, P. Stanley, G. W. Hart, M. Aebi, D. Mohnen, T. Kinoshita, N. H. Packer, J. H. Prestegard, R. L. Schnaar, P. H. Seeberger, Eds., *Essentials of Glycobiology* (Cold Spring Harbor Laboratory Press, ed. 4, 2022).
85. T. Robin, J. Mariethoz, F. Lisacek, Examining and fine-tuning the selection of glycan compositions with GlyConnect Compozitor. *Mol. Cell. Proteomics* **19**, 1602–1618 (2020).
86. L. R. L. Davies, A. Varki, Why is N-glycolylneuraminic acid rare in the vertebrate brain? *Top. Curr. Chem.* **366**, 31–54 (2015).
87. A. Hoffmann, M. Nimtz, U. Wurster, H. S. Conradt, Carbohydrate structures of β-trace protein from human cerebrospinal fluid: Evidence for "brain-type"N-glycosylation. *J. Neurochem.* **63**, 2185–2196 (1994).
88. Y.-J. Chen, D. R. Wing, G. R. Guile, R. A. Dwek, D. J. Harvey, S. Zamze, Neutral N-glycans in adult rat brain tissue. Complete characterisation reveals fucosylated hybrid and complex structures. *Eur. J. Biochem.* **251**, 691–703 (1998).
89. A. Hoffmann, M. Nimtz, R. Getzlaff, H. S. Conradt, "Brain-type" N-glycosylation of asialo-transferrin from human cerebrospinal fluid. *FEBS Lett.* **359**, 164–168 (1995).
90. S. Zamze, D. J. Harvey, Y.-J. Chen, G. R. Guile, R. A. Dwek, D. R. Wing, Sialylated N-glycans in adult rat brain tissue. A widespread distribution of disialylated antennae in complex and hybrid structures. *Eur. J. Biochem.* **258**, 243–270 (1998).
91. D. E. Sleat, I. Sohar, H. Lackland, J. Majercak, P. Lobel, Rat brain contains high levels of mannose-6-phosphorylated glycoproteins including lysosomal enzymes and palmitoyl-protein thioesterase, an enzyme implicated in infantile neuronal lipofuscinosis. *J. Biol. Chem.* **271**, 19191–19198 (1996).
92. D. R. Wing, T. W. W. Rademacher, M. C. C. Field, R. A. Dwek, B. Schmitz, G. Thor, M. Schachner, Use of large-scale hydrazinolysis in the preparation of N-linked oligosaccharide libraries: application to brain tissue. *Glycoconj. J.* **9**, 293–301 (1992).
93. I. J. Ji, S. Hua, D. H. Shin, N. Seo, J. Y. Hwang, I. S. Jang, M. G. Kang, J. S. Choi, H. J. An, Spatially-resolved exploration of the mouse brain glycome by tissue glyco-capture (TGC) and nano-LC/MS. *Anal. Chem.* **87**, 2869–2877 (2015).
94. R. U. Margolis, R. K. Margolis, D. M. Atherton, Carbohydrate-peptide linkages in glycoproteins and mucopolysaccharides from brain. *J. Neurochem.* **19**, 2317–2324 (1972).
95. Y. Naito-Matsui, L. R. L. Davies, H. Takematsu, H. H. Chou, P. Tangvoranuntakul, A. F. Carlin, A. Verhagen, C. J. Heyser, S. W. Yoo, B. Choudhury, J. C. Paton, A. W. Paton, N. M. Varki, R. L. Schnaar, A. Varki, Physiological exploration of the long term evolutionary selection against expression of N-glycolylneuraminic acid in the brain. *J. Biol. Chem.* **292**, 2557–2570 (2017).
96. O. O. Zaytseva, M. B. Freidin, T. Keser, J. Štambuk, I. Ugrina, M. Šimurina, M. Vilaj, T. Štambuk, I. Trbojević-Akmačić, M. Pučić-Baković, G. Lauc, F. M. K. Williams, M. Novokmet, Heritability of human plasma *N*-glycome. *J. Proteome Res.* **19**, 85–91 (2020).
97. L. A. Dworkin, H. Clausen, H. J. Joshi, Applying transcriptomics to study glycosylation at the cell type level. *iScience.* **25**, 104419 (2022).
98. C. Sisu, B. Pei, J. Leng, A. Frankish, Y. Zhang, S. Balasubramanian, R. Harte, D. Wang, M. Rutenberg-Schoenberg, W. Clark, M. Diekhans, J. Rozowsky, T. Hubbard, J. Harrow, M. B. Gerstein, Comparative analysis of pseudogenes across three phyla. *Proc. Natl. Acad. Sci. U.S.A.* **111**, 13361–13366 (2014).
99. S. Boellner, K.-F. Becker, Reverse phase protein arrays—Quantitative assessment of multiple biomarkers in biopsies for clinical use. *Microarrays.* **4**, 98–114 (2015).
100. Y. S. Okamoto, K. Omichi, S. Yamanaka, K. Ikenaka, S. Hase, Conversion of brain-specific complex type sugar chains by N-acetyl-β-D-hexosaminidase B. *J Biochem.* **125**, 537–540 (1999).
101. K. Angata, M. Fukuda, Polysialyltransferases: Major players in polysialic acid synthesis on the neural cell adhesion molecule. *Biochimie* **85**, 195–206 (2003).
102. U. Rutishauser, Polysialic acid in the plasticity of the developing and adult vertebrate nervous system. *Nat. Rev. Neurosci.* **9**, 26–35 (2008).
103. E. Ong, J. Nakayama, K. Angata, L. Reyes, T. Katsuyama, Y. Arai, M. Fukuda, Developmental regulation of polysialic acid synthesis in mouse directed by two polysialyltransferases, PST and STX. *Glycobiology.* **8**, 415–424 (1998).
104. H. Hildebrandt, C. Becker, M. Mürau, R. Gerardy-Schahn, H. Rahmann, Heterogeneous expression of the polysialyltransferases ST8Sia II and ST8Sia IV during postnatal rat brain development. *J. Neurochem.* **71**, 2339–2348 (1998).
105. E. Inoko, Y. Nishiura, H. Tanaka, T. Takahashi, K. Furukawa, K. Kitajima, C. Sato, Developmental stage-dependent expression of an α 2,8-trisialic acid unit on glycoproteins in mouse brain. *Glycobiology* **20**, 916–928 (2010).
106. N.-W. Lo, J. H. Shaper, J. Pevsner, N. L. Shaper, The expanding β4-galactosyltransferase gene family: Messages from the databanks. *Glycobiology* **8**, 517–526 (1998).
107. K. T. Schjoldager, Y. Narimatsu, H. J. Joshi, H. Clausen, Global view of human protein glycosylation pathways and functions. *Nat. Rev. Mol. Cell Biol.* **21**, 729–749 (2020).
108. Y. Narimatsu, H. J. Joshi, R. Nason, J. Van Coillie, R. Karlsson, L. Sun, Z. Ye, Y.-H. Chen, K. T. Schjoldager, C. Steentoft, S. Furukawa, B. A. Bensing, P. M. Sullam, A. J. Thompson, J. C. Paulson, C. Büll, G. J. Adema, U. Mandel, L. Hansen, E. P. Bennett, A. Varki, S. Y. Vakhrushev, Z. Yang, H. Clausen, An atlas of human glycosylation pathways enables display of the human glycome by gene engineered cells. *Mol. Cell* **75**, 394–407 (2019).
109. D. J. Harvey, G. R. Bousfield, Differentiation between sulphated and phosphated carbohydrates in low-resolution matrix-assisted laser desorption/ionization mass spectra. *Rapid Commun. Mass Spectrom.* **19**, 287–288 (2005).

Acknowledgments

Funding: This work was supported by the following funding sources: NIH grant MH124619 (N.S.), NIH grant MH116488 (N.S.), NIH grant DA053628 (N.S.), NIH grant R01HG010898-01 (N.S. and G.S.), Instituto de Salud Carlos III (Spain) grant MS20/00064 (G.S.), Agencia Estatal de Investigación (Spain) grant PID2019-104700GA-I00/AEI/10.13039/501100011033 (G.S.), and the European Union Seventh Framework Programme (FP7 2007 2013) under grant agreement no. 291823 Marie Curie FP7-PEOPLE-2011-COFUND (The New International Fellowship Mobility Programme for Experienced Researchers in Croatia NEWFELPRO). This paper has been written as a part of the project "A spatio-temporal analysis of glycosylation in the human brain (Human Neuroglycome)," which has received funding through NEWFELPRO project under grant agreement no. 34 (T.S.K.). We acknowledge the National Chimpanzee Brain Resource (funded by NIH NS092988) for contributing brain specimens used in this study. **Author contributions:** Conceptualization: T.S.K., I.G., G.L., and N.S. Formal analysis: G.S., F.V., S.M., S.B., A.K., A.C.N., and V.L. Investigation: T.S.K., I.G., M.N., I.B., R.R., and H.M.D. Resources: C.C.S., J.J.E., P.R.H., A.M.M.S., D.J., and N.S. Writing (original draft): T.S.K., I.G., and N.S. Writing (review and editing): T.S.K., I.G., G.S., A.M.M.S., C.C.S., P.R.H., G.L., and N.S. Visualization: T.S.K., I.G., G.S., F.V., S.M., N.S., and V.L. Supervision: G.L. and N.S. Project administration: G.L. and N.S. Funding acquisition: T.S.K., G.S., G.L., and N.S. **Competing interests:** The authors declare the following competing interests: G.L. is the founder and owner of Genos Ltd., a private research organization that specializes in high-throughput glycomic analysis and has several patents in this field. T.S.K., I.G., M.N., F.V., and I.B. are currently or were employees of Genos Ltd. while participating in this research project. These authors declare no other competing interests, and all other authors declare they have no competing interests. **Data and materials availability:** All data needed to evaluate the conclusions in the paper are present in the paper and/or the Supplementary Materials. Raw MS and MS/MS data are available from the GlycoPOST repository under the following accession numbers: rat (GPST000311), macaque (GPST000309), chimpanzee (GPST000310), adult human (GPST000308), and fetal human (GPST000312).

Submitted 12 December 2022
Accepted 7 November 2023
Published 6 December 2023
10.1126/sciadv.adg2615